Article

Structural mechanism of angiogenin activation by the ribosome

https://doi.org/10.1038/s41586-024-07508-8

Received: 8 November 2022

Accepted: 2 May 2024

Published online: 08 May 2024

Check for updates

Anna B. Loveland[1]✉, Cha San Koh[1], Robin Ganesan[2], Allan Jacobson[2] & Andrei A. Korostelev[1]✉

Angiogenin, an RNase-A-family protein, promotes angiogenesis and has been implicated in cancer, neurodegenerative diseases and epigenetic inheritance[1–10]. After activation during cellular stress, angiogenin cleaves tRNAs at the anticodon loop, resulting in translation repression[11–15]. However, the catalytic activity of isolated angiogenin is very low, and the mechanisms of the enzyme activation and tRNA specificity have remained a puzzle[3,16–23]. Here we identify these mechanisms using biochemical assays and cryogenic electron microscopy (cryo-EM). Our study reveals that the cytosolic ribosome is the activator of angiogenin. A cryo-EM structure features angiogenin bound in the A site of the 80S ribosome. The C-terminal tail of angiogenin is rearranged by interactions with the ribosome to activate the RNase catalytic centre, making the enzyme several orders of magnitude more efficient in tRNA cleavage. Additional 80S–angiogenin structures capture how tRNA substrate is directed by the ribosome into angiogenin's active site, demonstrating that the ribosome acts as the specificity factor. Our findings therefore suggest that angiogenin is activated by ribosomes with a vacant A site, the abundance of which increases during cellular stress[24–27]. These results may facilitate the development of therapeutics to treat cancer and neurodegenerative diseases.

Angiogenin was discovered as an angiogenesis factor required for vascularization[2] and, more recently, was found to have roles in other biological processes (reviewed previously[1]; see below). Angiogenin is upregulated in cancers, in keeping with the dependence of tumorigenesis on neovascularization[5–7]. By contrast, missense mutations in angiogenin are correlated with the development of neurodegenerative diseases such as amyotrophic lateral sclerosis (ALS), Parkinson's disease and Alzheimer's disease, highlighting the protein's key role in neuroprotection[8–10].

Angiogenin is a 14 kDa RNase-A-family ribonuclease, of which the RNase activity is required for angiogenesis, and is characterized by unusual properties[2,3]. First, despite its structural and sequence homology with the highly efficient RNase-A-like nucleases, purified angiogenin is at least 10,000-fold less active (k_{cat}/K_M) than RNase A[3,19,22]. The large difference between the catalytic activities of angiogenin and RNase A was proposed to correlate with the conformations of the C-terminal tails in protein structures[16,19,23]. The C terminus of catalytically competent RNase A adopts a β-sheet conformation that forms a substrate-binding surface containing the catalytic histidine corresponding to His114 in angiogenin[28]. By contrast, the C-terminal tail of free angiogenin (residues 116–123) folds into a short α-helix that partially occludes the substrate-binding site, consistent with the weak enzymatic activity of purified angiogenin[19,22]. Mutations of the C-terminal region that destabilize the α-helical fold increase the enzymatic activity of mutant angiogenin by 4–30-fold (refs. 17–19,29,30) and increase its angiogenic activity[17].

Second, angiogenin contrasts with the omnipotent RNase A in its high specificity toward tRNAs[11–14]. Angiogenin cleaves tRNAs in the anticodon stem loop, generating detectable 30- to 40-nucleotide-long tRNA fragments (also known as tRNA halves, tiRNAs and tsRNAs) and leading to potent inhibition of translation[11–15,31–33] and other downstream effects[34]. The tRNA-cleaving function of angiogenin is also implicated in transgenerational inheritance[4], stem cell maintenance[35] and astroglial support of motor neurons[36]. How angiogenin achieves high specificity towards tRNA in cells has been the subject of intense investigation. The catalytic activity of angiogenin substantially increases in cells and cell extracts[20,21]. Activation of angiogenin during cellular stress coincides with its colocalization with the translational machinery[37] and correlates with translation perturbation[38]. These observations suggest that the catalytic function of angiogenin may depend on the translational machinery.

To understand the mechanisms of angiogenesis activation and specificity, we studied how angiogenin interacts with the translation system. We found that the ribonuclease activity of angiogenin is potently activated by the mammalian 80S ribosome. Cryo-EM structures reveal the structural rearrangement of 80S-bound angiogenin into the RNase-A-like conformation, consistent with the enzyme's catalytic activation. Ribosomal positioning of the angiogenin active site next to newly delivered tRNAs underlies the angiogenin's specificity for the cleavage of tRNA anticodon stem loops. Thus, our research identifies the 80S ribosome as the activator and specificity factor for angiogenin.

[1]RNA Therapeutics Institute, UMass Chan Medical School, Worcester, MA, USA. [2]Department of Microbiology and Physiological Systems, UMass Chan Medical School, Worcester, MA, USA. ✉e-mail: anna.loveland@umassmed.edu; andrei.korostelev@umassmed.edu

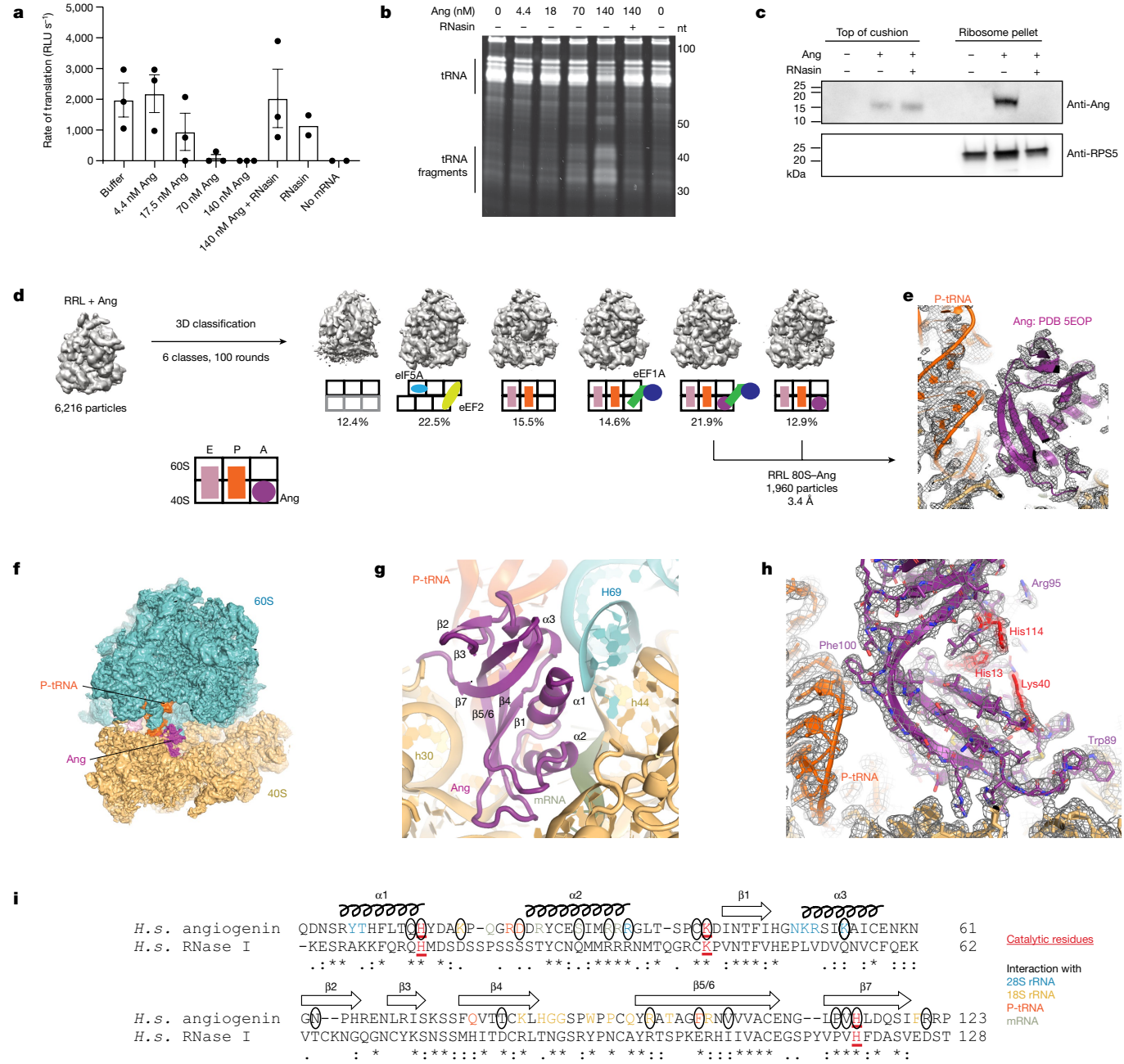

Fig. 1 | Angiogenin inhibits translation by binding to 80S ribosomes. **a**, Angiogenin (Ang) inhibits translation in RRL in a concentration-dependent manner. Inhibition is relieved by RNasin (RNase inhibitor). The apparent translation rate is shown (relative light units (RLU) s^{-1}). Data are mean ± s.e.m. $n = 2$ or 3 independent experiments, as shown. **b**, Incubation of RRL with angiogenin for 15 min leads to the accumulation of tRNA fragments; fragment accumulation is inhibited by RNasin. $n = 2$ independent experiments. nt, nucleotides. **c**, Angiogenin co-pellets with the ribosome fraction from RRL, except in the presence of RNasin. $n = 2$ independent experiments. **d**, Cryo-EM analysis of RRL with 1 μM angiogenin reveals that over 30% of 80S ribosomes have a novel density in the A site. **e**, Rigid-body fit of human angiogenin (PDB: 5EOP)[61] into the 3.4 Å cryo-EM map of angiogenin-bound ribosomes in RRL. **f**, A 3.0 Å cryo-EM map of in vitro assembled 80S–angiogenin complex. The 60S subunit is coloured cyan; 40S subunit is coloured yellow; P-site tRNA is coloured orange; mRNA is coloured green; angiogenin is coloured magenta. **g**, Angiogenin in the A-site of the ribosome with the secondary structure labelled. **h**, Cryo-EM density showing well-resolved interactions of angiogenin with P-tRNA and 18S rRNA; the three catalytic residues are shown in red. C-terminal residues of angiogenin (118 to 123) and h30 have been omitted to show P-tRNA interactions. The mesh shows a 2.8 Å cryo-EM map with *B*-factor sharpening of −50 $Å^2$. **i**, Sequence alignment of human angiogenin with human RNase I; the secondary structure is indicated for angiogenin in the ribosome complex, including β-strand 5 joining β-strand 6 (5/6) and β-strand 7. The underlined red letters indicate catalytic residues[16,23]. The blue letters indicate angiogenin residues adjacent to 28S rRNA. The gold residues are adjacent to 18S rRNA. The green residues are adjacent to mRNA. The orange residues are adjacent to P-site tRNA. Residues with mutations associated with ALS and Parkinson's disease are indicated by circles[8–10]. *H.s.*, *Homo sapiens*.

Angiogenin rearranges after 80S binding

To investigate how angiogenin inhibits translation, we tested the effect of angiogenin on a mammalian translation system. Consistent with previous reports[14,32], translation in different preparations of rabbit reticulocyte lysates (RRL) was inhibited by 20–70 nM human angiogenin (Fig. 1a). Addition of angiogenin to RRL resulted in the depletion of full-length tRNA and the appearance of 30–40-nucleotide

RNA fragments, consistent with tRNA cleavage (Fig. 1b) as previously reported[11,13,14]. Inhibition of angiogenin by RNasin[39], a commercial version of the protein human ribonuclease/angiogenin inhibitor 1, restored translation and prevented the accumulation of tRNA fragments (Fig. 1a,b), indicating that RNasin may block the interaction of angiogenin with its activating molecule and/or substrate.

We next tested whether angiogenin interacts with the lighter (such as individual proteins or RNA) or heavier (such as ribosomes) components of the translation system. Sucrose-cushion ultracentrifugation revealed that angiogenin is present in the ribosome fraction (Fig. 1c). Addition of RNasin prevents association with the heavier fraction, suggesting that angiogenin function may depend on its interaction with the ribosome.

To visualize possible interaction(s) between angiogenin and the ribosome in the context of an active translation system, we collected a cryo-EM dataset of an RRL reaction with angiogenin (Fig. 1d). Owing to the high macromolecular content of the lysate, the micrographs were noisy and had low contrast. Nevertheless, distinguishable 80S ribosomes in the best images (Methods and Extended Data Fig. 1a,b) could be computationally classified, yielding six cryo-EM maps with a resolution of approximately 4 Å, representing the dominant ribosome states in the RRL reaction (Fig. 1d and Extended Data Table 1). Notably, two classes representing around 30% of 80S particles had a novel density in the ribosomal decoding centre (40S A site); one of the maps contained additional density representing the eEF1A–tRNA complex near the A site. The local resolution was low, probably due to the compositional heterogeneity of ribosome complexes (for example, different tRNAs and mRNA positions) of the ribosomes. Nevertheless, rigid-body fitting shows that the novel density is consistent with human angiogenin bound to the ribosome (Fig. 1e and Extended Data Fig. 2a).

To improve the compositional homogeneity of the complex and the resolution of the maps, we reconstituted the 80S–mRNA–tRNA–angiogenin complex using available, purified components and performed cryo-EM analysis. Relying on the high conservation of translation machinery, our ribosome complex contained rabbit 40S and 60S ribosomal subunits, a synthetic leaderless mRNA encoding AUG positioned in the P site and UUC in the A site, bacterial initiator $tRNA^{fMet}$ efficiently binding to the mammalian ribosomal P site[40] and recombinantly expressed human angiogenin (Methods). Cryo-EM data classification revealed that more than 50% of ribosomes bound to angiogenin. A 3.0-Å-resolution cryo-EM map shows a well-resolved angiogenin bound to the A site of the small (40S) subunit of the ribosome (Fig. 1f, Extended Data Fig. 1c,d and Extended Data Table 1). Maximum-likelihood classification of cryo-EM data revealed that, among numerous ribosomal and tRNA conformations reflecting distinct functional states, angiogenin is bound only with the elongation-like ribosomes containing P-site tRNA (Extended Data Fig. 1c), echoing the finding in the RRL dataset. Approximately 2,200 $Å^2$ (around 30%) of angiogenin's solvent accessible surface area interacts with the ribosome, indicating strong and specific binding[41]. Angiogenin interacts through polar and hydrophobic groups with all elements of the decoding centre, including 28S rRNA, 18S rRNA, mRNA and the adjacent P-tRNA (Fig. 1g,h).

Helices α1 and α3 of angiogenin bind to the central helix 69 (H69) of 28S rRNA, which docks into the decoding centre of the small subunit (Fig. 1g). The positively charged patch of α3, composed of Lys50, Arg51 and Lys54 binds to the phosphodiester backbone of H69 (Extended Data Fig. 1e). These residues are specific to angiogenin (for example, human RNase I, also known as pancreatic RNase or RNase A, features short uncharged side chains), in keeping with their role in ribosome binding (Fig. 1i; see also the next section). Interactions with 18S rRNA are predominately formed by strands β4 and β5/6 and their connecting loop (amino acids 76–101) (Extended Data Fig. 1f). Trp89 stacks onto 18S nucleotide U627 (U531 in *Escherichia coli*), a key element of the ribosomal decoding centre near the mRNA-binding tunnel (Extended Data Fig. 1f). Arg33 of α2 bridges the two ribosomal subunits by reaching into the decoding centre toward universally conserved nucleotides A3760 at the tip of H69 (corresponding to A1913 in *E. coli* 23S rRNA) and A1825 of the small-subunit helix 44 (h44; A1493 in *E. coli* 16S rRNA) (Extended Data Fig. 1g). α2 is adjacent to the A-site mRNA codon, where Arg24 stacks on the first nucleotide of the codon (Extended Data Fig. 1h,j). Lastly, angiogenin contacts the backbone of P-site tRNA by the stacking of Phe100 onto the ribose of the tRNA's nucleotide 28, while Gln77 reaches the phosphate group of this nucleotide (Fig. 1h and Extended Data Figs. 1i and 2a). Backbone interactions at this position of P-tRNA are probably insensitive to tRNA identity and indeed are also seen in the cryo-EM map directly from RRL (Extended Data Fig. 2a). Extensive interactions with the ribosomal decoding centre, mRNA and P-site tRNA suggest that angiogenin specifically binds to elongating ribosomes of which the A site is vacant (that is, not occupied by tRNA or another ligand), which may accumulate due to ribosome stalling or cellular stress[24–27]. The ribosome-binding activity of angiogenin may explain loss-of-function mutations that were not previously explained by angiogenin's cell-receptor binding[42], nuclear localization[43] or RNase activity or other processes[44,45]. For example, many ribosome interactions involve angiogenin's surface residues of which mutations are associated with ALS and Parkinson's disease[8–10] (Fig. 1i).

Angiogenin's conformation is altered by ribosome binding, suggesting a mechanism for the catalytic activation of the enzyme (Fig. 2). The activity of free angiogenin is several orders of magnitude lower than that of RNase A[3,19,22] (Fig. 2c (left)), and the α-helical conformation of the C-terminal tail of angiogenin was proposed to be inhibitory because it occludes substrate binding[17–19,29,30] (Fig. 2c (middle)). In the 80S–angiogenin ribosome complex, the C terminus of angiogenin is shifted by more than 15 Å and rearranged to extend β-strand 7 (Fig. 2c (right)), similar to that in free RNase A (Fig. 2c (left)). In this conformation, the C terminus is stabilized by interactions with the minor groove of 18S rRNA helix 30 (h30) and the neighbouring β-strands 5 and 6, which are reorganized into a single longer stand that we term β5/6 (Fig. 2c). Here, Phe120 of angiogenin packs between A1522 of h30 and Arg101 of β5/6 docked at the phosphate group of C1237, while the neighbouring Ile119 binds near the C terminus of uS19 (Fig. 2d and Extended Data Fig. 2a). In this rearranged angiogenin conformation, the substrate-binding site is open and catalytic residues His13 and His114 are positioned to catalyse substrate cleavage as in RNase A (Fig. 2c). The active site is exposed in the intersubunit space and is fully accessible to tRNA substrates (Fig. 2a), as seen in the cryo-EM maps from RRL in which ternary complex places the tRNA's anticodon next to angiogenin's active site (Extended Data Fig. 2a).

Ribosome activates angiogenin's nuclease

To test whether the ribosome directly activates angiogenin's RNase activity, we compared the ability of angiogenin alone or together with various ribosome complexes to cleave tRNA. We first tested in vitro transcribed yeast $tRNA^{Ala}$, of which the anticodon loop is identical to that of human $tRNA^{Ala}$, which is known to generate inhibitory tRNA fragments[12] (Fig. 2e–g). We used a low concentration (10 nM) of angiogenin commensurate with the affinities of bona fide translation factors, such as eRF1–eRF3 and eEF2, that bind to the ribosomal A site[46,47]. With angiogenin alone, no $tRNA^{Ala}$ cleavage was detected after 100 min (Fig. 2f,g (lane 3)), consistent with previous reports of poor activity of isolated angiogenin[3,19,22]. By contrast, within 1 min of adding $tRNA^{Ala}$ to a reaction containing 10 nM angiogenin and 20 nM 80S elongation ribosome complex, ~35-nucleotide tRNA fragments began to accumulate and, after 100 min, we detected more than 100-fold accumulation of cleavage products (Fig. 2f,g (lanes 7 and 9)).

Similarly, in the presence of the 80S complex, angiogenin potently cleaved endogenous mammalian tRNAs purified from RRL (Extended Data Fig. 2b). Northern blotting identified the fragments of $tRNA^{Asp}$, $tRNA^{Gly}$ and $tRNA^{His}$ (Extended Data Fig. 2b), which were shown to be

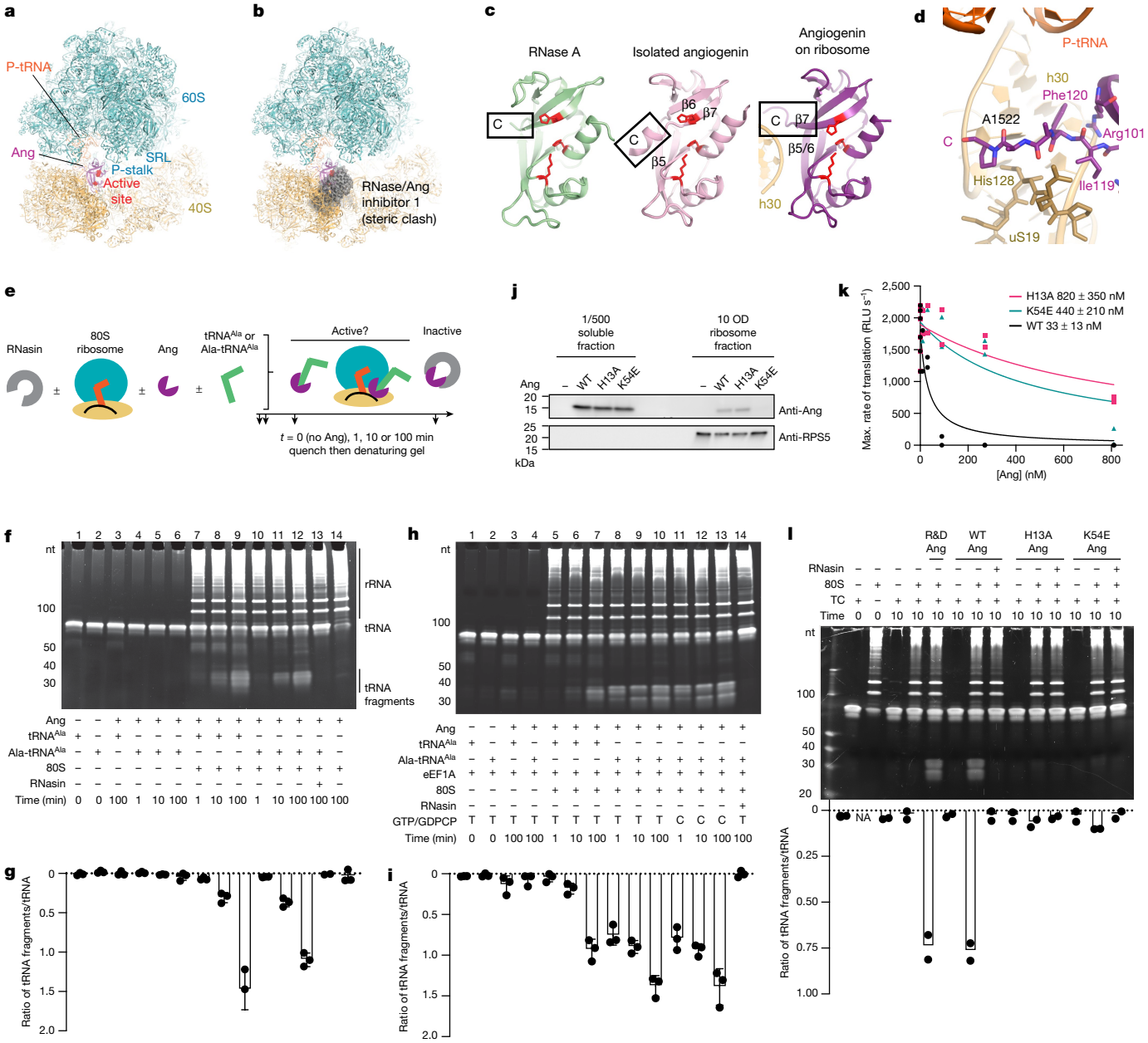

Fig. 2 | Angiogenin's RNase is activated after ribosome binding. a, The catalytic residues (red spheres) of angiogenin face the tRNA-delivery path, comprising the tRNA-binding P-stalk and SRL of the 60S subunit. **b**, Interaction between angiogenin and the ribosome is incompatible with angiogenin's interaction with the RNase/Ang inhibitor 1 (grey) due to steric clash. Structural alignment compares ribosome-bound angiogenin with angiogenin bound to human RNase/Ang inhibitor 1 (PDB: 1A4Y)[39]. **c**, Catalytically active RNase A contains a C-terminal β-strand (left; PDB: 5RSA)[28], whereas isolated angiogenin has an inhibited α-helical C terminus (middle; PDB:5EOP)[61]. Ribosome-bound angiogenin features a β-strand C terminus (right; this study) like RNase A. **d**, The C-terminal β-strand of angiogenin is stabilized by ribosomal h30 of 18S rRNA, uS19 and the β5/6 strand. **e**, Schematic of the measurement 80S-stimulated tRNA cleavage by angiogenin, showing the order of addition of components from left to right. **f**, Urea–PAGE gel showing that the production of tRNA fragments by 10 nM angiogenin (R&D) is stimulated by the 80S ribosome. **g**, The ratio of signals of tRNA fragments to full-length tRNAs. Data are mean ± s.d. $n = 3$ independent experiments. **h**, The production of tRNA fragments by ribosome-bound angiogenin is further stimulated by eEF1A ternary complex with GTP (T) or GDPCP (C) and Ala-tRNA^{Ala}. **i**, The ratio of signals from tRNA fragments to full-length tRNA. Data are mean ± s.d. $n = 3$ independent experiments. **j**, WT and H13A, but not K54E, angiogenin co-pellets with ribosomes from RRL supplemented with 1 μM of each angiogenin. $n = 2$ independent experiments. Western blot analysis of the supernatant and ribosome pellet is shown. OD, optical density units at 260 nm. **k**, The concentration dependence of translation inhibition in RRL by WT, H13A or K54E angiogenin. IC_{50} values are shown. $n = 2$ independent experiments. **l**, Comparison of ribosome-stimulated tRNA cleavage (in a ternary complex of eEF1A–GDPCP–Ala-tRNA^{Ala}) by R&D angiogenin and refolded WT, H13A or K54E angiogenin. NA, not applicable. Data are the mean of $n = 2$ independent experiments.

angiogenin substrates in previous studies[12,31,38]. RNasin prevented tRNA cleavage in the presence of the 80S complex (Fig. 2f,g (lane 13) and Extended Data Fig. 2b), consistent with RNasin's ability to block angiogenin's binding to the ribosome (Fig. 1c). Indeed, angiogenin's helices α1 and α3, which interact with the ribosomal H69 and P-site tRNA, are occluded in the complex of angiogenin with human ribonuclease/angiogenin inhibitor 1 (RNase/Ang inhibitor 1)[39]. Furthermore, the angiogenin–RNase/Ang inhibitor 1 complex is incompatible with ribosome binding due to a severe clash of RNase/Ang inhibitor 1 with the 40S subunit (Fig. 2b). Thus, the 80S ribosome potently stimulates

tRNA cleavage into ~35-nucleotide fragments by angiogenin, consistent with the cryo-EM structure described above.

We next examined whether the translation elongation factor eEF1A, which delivers aminoacyl-tRNA to the ribosome during translation elongation in cells, efficiently presents tRNA to the 80S–angiogenin complex for cleavage. The tRNA cleavage assay revealed that eEF1A further stimulates tRNA cleavage of amino-acylated $tRNA^{Ala}$ by ribosome-bound angiogenin, resulting in faster accumulation of tRNA fragments than that without eEF1A (compare the 1 min timepoints, at which a 10- to 100-fold higher accumulation of tRNA fragments occurs; Fig. 2h,i (lane 8) versus Fig. 2f,g (lane 10)). By contrast, eEF1A did not stimulate deacyl-tRNA cleavage, consistent with the inability of eEF1A to bind to deacyl-tRNA[48] (Fig. 2h,i (lane 5)). Although GTP hydrolysis on eEF1A is required for elongation[48], eEF1A stimulated amino-acylated tRNA cleavage similarly in the presence of either GTP or the non-hydrolysable GTP analogue GDPCP (Fig. 2h,i (lane 8 versus lane 11)). These results suggest that eEF1A binding to the ribosome results in optimal presentation of tRNA to the angiogenin catalytic site, but hydrolysis of GTP by eEF1A is not required for tRNA cleavage.

We tested whether perturbations of angiogenin's catalytic activity and ribosome binding would reduce tRNA cleavage and translation inhibition. We characterized a catalytically compromised angiogenin mutant H13A[23,49] and a disease-associated mutation K54E[45,50], which is predicted to disrupt angiogenin's interaction with the ribosomal H69 (Methods and Extended Data Figs. 1e and 3a,e–g). Indeed, sucrose-cushion ultracentrifugation of translating RRL or stalled ribosomes with angiogenin shows that wild-type (WT) angiogenin and angiogenin(H13A) associate with the ribosome fraction, whereas angiogenin(K54E) association with ribosomes is much weaker (Fig. 2j and Extended Data Fig. 3b). Accordingly, the catalytically inactive angiogenin(H13A) (half-maximum inhibitory concentration (IC_{50}) of 820 ± 350 nM) and the ribosome-binding deficient angiogenin(K54E) (IC_{50} of 440 ± 210 nM) mutants inhibit translation at concentrations an order of magnitude higher than the WT enzyme (IC_{50} of 33 ± 13 nM) (Fig. 2k and Extended Data Fig. 3c,i,j). This is consistent with the inefficient tRNA cleavage by these mutant proteins in the presence of the ribosome (Fig. 2l and Extended Data Fig. 3d,h). Lastly, we find that that the related and highly active pancreatic RNase A[3,19,22] does not associate with the ribosome fraction (Extended Data Fig. 3b), consistent with the divergence of ribosome-interacting residues on the surfaces of RNase A and angiogenin (Fig. 1i). This further emphasizes the unique dependence of angiogenin on ribosome binding for its catalytic activation.

We tested how angiogenin activation depends on the ribosomal subunit, tRNA and mRNA occupancies. 40S ribosomal subunits did not activate angiogenin cleavage (Extended Data Fig. 4a,b (lane 6)). 60S subunits showed very weak stimulatory activity possibly due to 80S contamination; consistent with this idea, our examination of individual 60S subunits in cryo-EM data did not reveal angiogenin binding (Methods and Extended Data Fig. 4a,b (lane 10)). These observations indicate that the 80S ribosome is required for angiogenin activation and fast tRNA cleavage, in agreement with cryo-EM structures showing angiogenin interacting with both subunits (Fig. 1g). The absence of mRNA or cognate P-site tRNA (Extended Data Fig. 4f (lanes 3–5 and 7–9)) slowed tRNA cleavage relative to the elongation-like 80S complex (Extended Data Fig. 4f (lanes 11–13)), in keeping with the structure of the activated angiogenin interacting with both the mRNA and P-tRNA (Fig. 1g). The identity of the codon in the A site had a mild effect on cleavage activity in experiments including four model mRNAs (Extended Data Fig. 4f). We tested all-pyrimidine (UUC), all-purine (AAA), mixed (UAA) and truncated (U) A-site mRNA compositions. 80S with the mRNA used in the cryo-EM complex (Fig. 1f–h), encoding phenylalanine (UUC), and with an mRNA encoding a stop codon (UAA) yielded similarly fast tRNA cleavage (Extended Data Fig. 4f (lanes 11–13 and 18–20)). A lysine codon (AAA)—which, in contrast to UUC and UAA, contains a purine at the first position—showed less cleavage at the 1 min timepoint but reached a similar end point, indicating a moderately slower reaction (Extended Data Fig. 4f (lanes 22–24)). Truncated mRNA containing a single uridine residue in the A site also allowed for tRNA cleavage (Extended Data Fig. 4f (lanes 26–28)). Thus, activation of angiogenin occurs on 80S ribosome complexes and can moderately depend on mRNA codon identity, consistent with the high fraction of 80S ribosomes (~30%) bound by angiogenin in cell lysates (Fig. 1d).

Ribosome directs tRNA to angiogenin

To understand how tRNA is delivered and positioned for cleavage by ribosome-bound angiogenin, we used cryo-EM to analyse the reconstituted 80S–angiogenin complex supplemented with eEF1A–Ala-$tRNA^{Ala}$–GDPCP ternary complex. Maximum-likelihood classification of the cryo-EM dataset revealed three types of ribosome complexes bound to angiogenin (Extended Data Figs. 5a,b and 6 and Extended Data Table 1): (1) 80S–angiogenin, as described above, at an improved average resolution of 2.8 Å (Fig. 1h; a minor fraction of partially rotated ribosomes with P-site tRNA is described in the Methods); (2) 80S–angiogenin with eEF1A and Ala-$tRNA^{Ala}$ at 3.7 Å average resolution (Fig. 3a and Extended Data Fig. 6); and (3) 80S–angiogenin with $tRNA^{Ala}$ at 3.1 Å average resolution (Fig. 3b and Extended Data Fig. 6). The tRNA-bound ribosome particles represent only a fraction (<20%) of angiogenin-bound ribosomes, consistent with transient interactions between the incoming tRNA and activated enzyme in the multiple-turnover reaction. In both complexes containing $tRNA^{Ala}$, the anticodon loop was unresolved, suggesting that the maps contain the products of fast tRNA cleavage (Extended Data Fig. 6d,e,g,h). Indeed, PAGE analysis of the cryo-EM reaction shows that $tRNA^{Ala}$ is cleaved (Extended Data Fig. 5e).

In the structure with eEF1A and Ala-$tRNA^{Ala}$, the ternary complex is placed around 22 Å farther from the A site than during decoding (as measured at U47 of Ala-$tRNA^{Ala}$ to equivalent U48 of $tRNA^{Val}$ of the mammalian decoding complex; Protein Data Bank (PDB): 5LZS)[51], because the A site is occupied with angiogenin (Fig. 3c,d). The phosphate of the last modelled tRNA nucleotide of the anticodon stem (U38) is placed near the active site of angiogenin, consistent with catalytic cleavage near this position (Fig. 3c). Indeed, based on the preference of angiogenin to cleave between a pyrimidine and an adenosine residue[52], the anticodon loop of $tRNA^{Ala}$ (^{32}UUAGCAU^{38}) may be cleaved after positions 33 and 36 (Extended Data Fig. 4c–e). The canonical L-shaped structure of tRNA is present (Extended Data Fig. 6j) except for the anticodon loop (Extended Data Fig. 6d,g), indicating that cleavage does not disrupt the overall fold of tRNA. Two major contacts hold the tRNA in place: the elbow interacts with the 28S rRNA of the dynamic P stalk (at nucleotide G19 of $tRNA^{Ala}$ and A2009 of 28S rRNA), similarly to the interaction observed during mRNA decoding[51]; and the acceptor arm of tRNA binds to eEF1A, which is docked on the 40S ribosomal subunit around 10 Å away from the sarcin-ricin loop (SRL) of the large subunit (Fig. 3c,e). This placement of eEF1A away from the SRL—the site of GTPase activation in mRNA-decoding complexes[51,53]—agrees with our observation that GTP hydrolysis is not required for tRNA cleavage by ribosome-bound angiogenin.

In comparison to eEF1A-bound tRNA, deacyl-tRNA in the 80S–angiogenin–$tRNA^{Ala}$ structure shifts outward by more than 4 Å (Fig. 3e). The cleaved tRNA is placed slightly differently than in the eEF1A-containing map (Fig. 3e and Extended Data Fig. 6). While the anticodon stem of tRNA is placed near angiogenin, the elbow is held further out by the P stalk. Subclassification of the cryo-EM density corresponding to this complex suggests several positions of the P stalk and the tRNA, differing by up to 8 Å at the tip of the acceptor arm (Fig. 3e and Supplementary Videos 1 and 2). The flexible tethering of tRNA by the P stalk may allow access of different nucleotides within the anticodon loop to angiogenin's active site, accounting for cleavage of various or possibly all tRNA species with consensus nucleotide sequences[31,33,38]. The flexible tethering contributes to the lower resolution of the cryo-EM

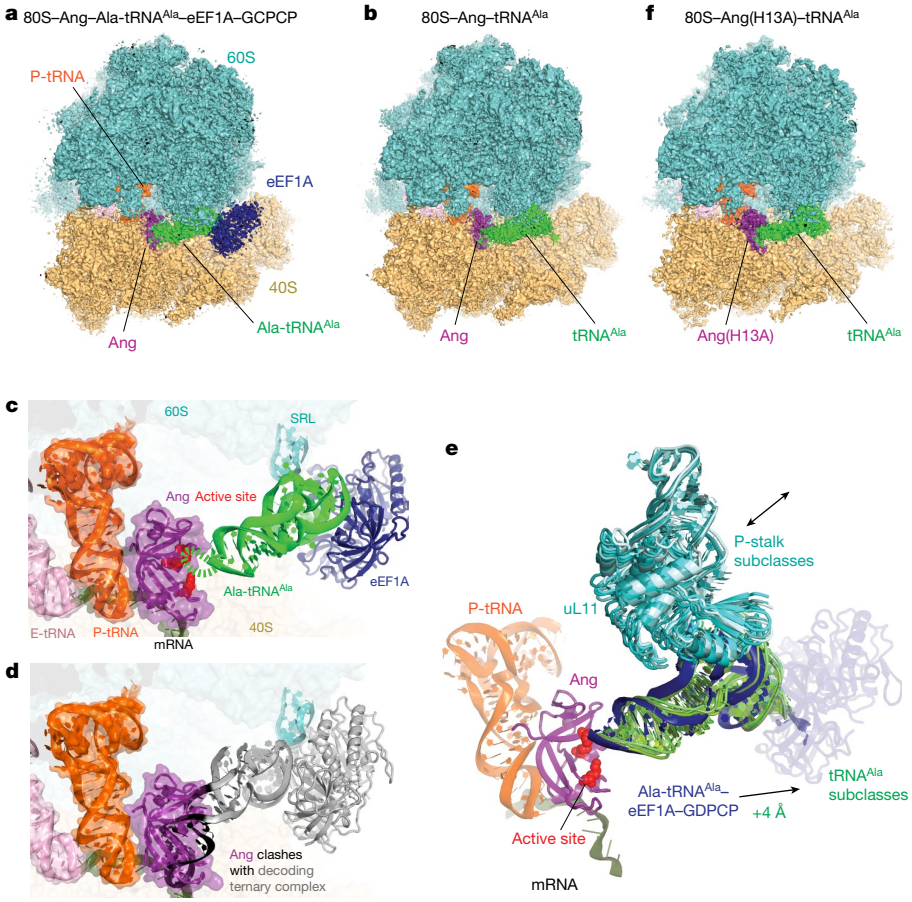

Fig. 3 | Cryo-EM structures of 80S–angiogenin complexes formed with eEF1A–GDPCP and tRNA. a, A 3.7 Å cryo-EM map of 80S–angiogenin bound to eEF1A–Ala-tRNA^{Ala}, coloured as in Fig. 1 with the addition of green for Ala-tRNA^{Ala} and dark blue for eEF1A. **b**, A 3.1 Å cryo-EM map of 80S–angiogenin bound to tRNA^{Ala}. **c**, The anticodon stem of Ala-tRNA^{Ala} (green) in the ternary complex is next to the angiogenin active site (red spheres), but the anticodon loop is not resolved due to cleavage and/or mobility (dashed green line). **d**, The anticodon stem of tRNA decoding mRNA (grey; from PDB: 5LZS)[51] clashes with angiogenin (clashing residues are black), highlighting that angiogenin binding is incompatible with mRNA decoding. **e**, Different positions for tRNA^{Ala} among five different cryo-EM maps suggest tRNA mobility near angiogenin. The 60S P-stalk (shades of cyan) and tRNA (shades of green) exhibit different positions between classes indicative of ~8 Å movement. **f**, A cryo-EM map of 80S–angiogenin(H13A) bound with tRNA^{Ala}.

density for tRNA^{Ala} as compared to angiogenin, necessitating the use of low-pass-filtered maps for the fitting of eEF1A-bound and deacylated tRNA models (Extended Data Fig. 6g–l). The 3′-CCA end is close to or docked at 18S rRNA helix 5 (h5) near residue Ala50 (Extended Data Fig. 6k and Supplementary Video 2). This interaction is sterically incompatible with binding of eEF1A, suggesting that this structure may represent a deacylated tRNA that initially bound the ribosome without eEF1A. Thus, the cryo-EM structures with tRNA^{Ala} show how ribosome-bound angiogenin can bind to and cleave tRNAs, whether or not they are delivered by eEF1A, consistent with our biochemical observations (Fig. 2f–i).

We next characterized the catalytically compromised angiogenin(H13A) mutant[23,49] (Fig. 2j,l, Extended Data Fig. 3 and Extended Data Table 1) to test whether it binds to the ribosome similarly to WT protein and how an incoming tRNA interacts with the active site before cleavage. In the 2.8 Å cryo-EM map of the 80S complex (Fig. 3f), the fold and active site of the angiogenin(H13A) variant is nearly identical to WT angiogenin except for the expected difference in the angiogenin(H13A) side chain (Extended Data Fig. 6c). Density for the tRNA's anticodon stem–loop near the active site is more continuous than that in the WT angiogenin complex (Extended Data Fig. 6f,i), consistent with the uncleaved tRNA substrate observed in the PAGE analysis of the cryo-EM sample (Extended Data Fig. 5f). As in the WT angiogenin complex, the overall resolution of the tRNA is lower than that of the rest of structure, suggesting that the substrate attached to the mobile P stalk is also conformationally dynamic. In summary, experiments with the angiogenin(H13A) mutant underscore that tRNA cleavage occurs on the ribosome-bound angiogenin with tRNA presented to the active site by the P-stalk and that tRNA cleavage is required for translation inhibition by angiogenin (Fig. 2k and Extended Data Fig. 3c,i,j).

To test whether the overall tRNA fold and tRNA interactions with the ribosome are important for angiogenin's substrate specificity, we tested the cleavage of (1) a short 17-nucleotide hairpin representing the anticodon stem–loop of tRNA^{Ala} and (2) a 30-nucleotide hairpin, similar in length to the tRNA anticodon domain including the D stem, which therefore might contact the P stalk if bound to the ribosome (Extended Data Fig. 2c). Neither of these hairpins could be cleaved by angiogenin in a complex with the ribosome, indicating that the overall tRNA structure and ribosomal interactions are required for the efficient cleavage by ribosome-bound angiogenin. These findings further emphasize that the exquisite substrate specificity of angiogenin is provided by the ribosome.

Conclusions

Elucidating the function and therapeutic potential of angiogenin requires an understanding of the molecular mechanism of angiogenin activation. Our work shows that angiogenin is activated by 80S

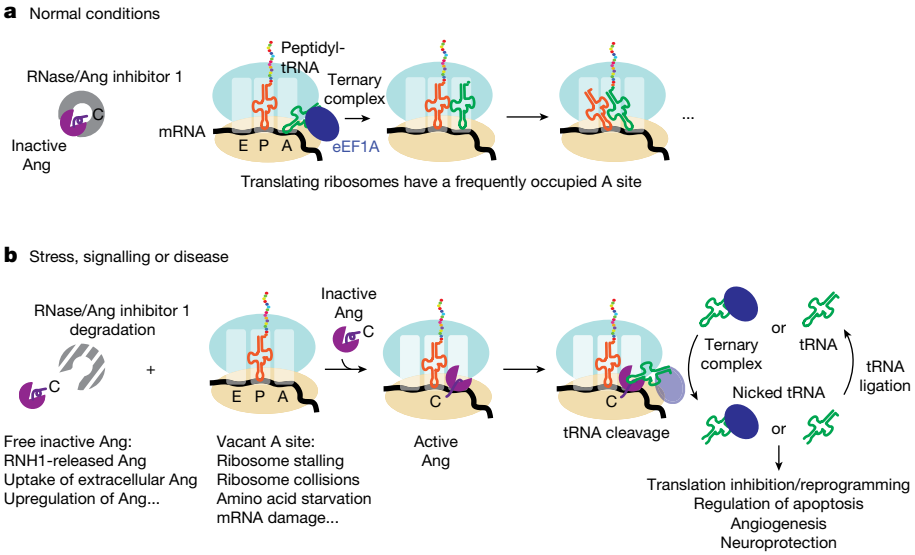

Fig. 4 | Schematic of angiogenin activation and specificity toward tRNA induced by the 80S ribosome. a, Under normal conditions, angiogenin is inhibited by RNase/Ang inhibitor 1, and active translation keeps the 80S ribosomal A sites mostly occupied. **b**, Cellular stress, intercellular signalling or diseases such as cancer can lead to degradation of RNase/Ang inhibitor 1 and/or an increase of free, inactive angiogenin, but the RNase activity of angiogenin is still limited by its inactive C terminus. Cell stress or disease can also cause the accumulation of 80S ribosomes with vacant A-sites, allowing angiogenin to bind and become activated by the refolding of C-terminal residues. Free or eEF1A-bound tRNAs, which are presented by the ribosome to angiogenin's active site, are efficiently cleaved at the anticodon loop. This cleavage inhibits translation. Nicked tRNAs may affect other downstream processes or be unwound into tRNA halves or fragments to carry out their many roles in translation inhibition, apoptosis, angiogenesis and neuroprotection. Nicked tRNAs may also be returned to the tRNA pool, for example, by the RNA ligase RtcB.

cytoplasmic ribosomes with a vacant A site (Fig. 4). Such ribosome species accumulate during cellular stresses[24–27] (Supplementary Discussion). In cells, the interaction between angiogenin and ribosomes must occur after the stress-induced degradation[54] or downregulation[38] of RNase/Ang inhibitor 1, the gene product of *RNH1* (Fig. 4b), which normally prevents the catalytic activity of angiogenin by occluding the angiogenin active site[39] and by sterically blocking angiogenin from ribosome binding (Fig. 2b). Ribosome binding is required for efficient tRNA cleavage and translation inhibition, as emphasized by the disease-associated mutation K54E disrupting ribosome binding and angiogenin activation (Fig. 2j–l). Interaction between angiogenin and the ribosome stabilizes angiogenin's C terminus in a catalytically active RNase-A-like conformation (Fig. 2c), consistent with previous mutational and structural analyses that suggested that C-terminal rearrangement is required for catalysis[16–19,29,30]. The active site of angiogenin is directed toward incoming tRNA substrates (Fig. 3). In cells, tRNAs are commonly bound within the eEF1A ternary complex with GTP (and are aminoacylated) or are deacylated. We show that both aminoacylated and deacylated tRNAs are substrates for ribosome-bound angiogenin (Fig. 2). Incoming tRNAs are flexibly held by the ribosomal P-stalk, with the anticodon loop presented at the angiogenin active site resulting in the rapid cleavage of tRNA (Fig. 3e). This structural mechanism accounts not only for the activation of angiogenin, but also for the substrate specificity provided by the ribosome, of which the P stalk is tuned for tRNA delivery. Angiogenin was proposed to also cleave the 3′ CCA ends of tRNA[55]; however, recent genetic and tRNA sequencing analyses argue that angiogenin does not have the CCA-cleaving activity and that another RNase could be responsible for the 3′ cleavage[33]. In our structures, the CCA ends of tRNA bind more than 70 Å away from angiogenin's active site (Fig. 3), in keeping with angiogenin's selective cleavage of the anticodon loops.

Notably, the resulting nicked tRNA is held together by nucleotide stacking interactions at tRNA stems and retains the overall tertiary structure of tRNA (Fig. 3 and Extended Data Fig. 6j–l), as opposed to separated single-stranded tRNA 'fragments' that are often implicated in downstream functions[34]. Thus, angiogenin-mediated tRNA cleavage could inhibit translation by depleting functional tRNAs and/or by producing non-productive stalled complexes of nicked tRNAs with tRNA-interacting molecules, such as ribosomes and tRNA-binding enzymes (Fig. 4). Indeed, the accumulation of nicked tRNAs may occur under stress conditions without strand separation[56,57] and is counteracted by the repair enzyme RtcB, which ligates nicked tRNA[57,58]. Alternatively, nicked tRNAs can be processed or unwound by helicases to form tRNA fragments[59]. The nicking or fragmentation of tRNA by angiogenin is implicated in many processes, including global translation inhibition[12], apoptosis repression[60], stem cell maintenance[35], transgenerational inheritance[4], astroglial support of motor neurons[36] and other roles in the central nervous system[8–10]. The molecular targets of fragmented/nicked tRNAs in these processes remain to be fully elucidated, but our and others' data show that translation is a major inhibited pathway[11,12,15]. Indeed, angiogenin-catalysed tRNA cleavage inhibits translation, whereas the catalytically inactive angiogenin(H13A) mutant, which retains ribosome binding, does not affect translation under similar conditions (Fig. 2k). Future research will continue to investigate the downstream effects of the tRNA-like cleavage products and will explore therapeutic routes to targeting the ribosome-driven activation of angiogenin.

Online content

Any methods, additional references, Nature Portfolio reporting summaries, source data, extended data, supplementary information, acknowledgements, peer review information; details of author contributions and competing interests; and statements of data and code availability are available at https://doi.org/10.1038/s41586-024-07508-8.

1. Sheng, J. & Xu, Z. Three decades of research on angiogenin: a review and perspective. *Acta Biochim. Biophy. Sin.* **48**, 399–410 (2016).
2. Fett, J. W. et al. Isolation and characterization of angiogenin, an angiogenic protein from human carcinoma cells. *Biochemistry* **24**, 5480–5486 (1985).

3. Shapiro, R., Riordan, J. F. & Vallee, B. L. Characteristic ribonucleolytic activity of human angiogenin. *Biochemistry* **25**, 3527–3532 (1986).
4. Zhang, Y. et al. Angiogenin mediates paternal inflammation-induced metabolic disorders in offspring through sperm tsRNAs. *Nat. Commun.* **12**, 6673 (2021).
5. Hartmann, A. et al. Hypoxia-induced up-regulation of angiogenin in human malignant melanoma. *Cancer Res.* **59**, 1578–1583 (1999).
6. Yoshioka, N., Wang, L., Kishimoto, K., Tsuji, T. & Hu, G.-F. A therapeutic target for prostate cancer based on angiogenin-stimulated angiogenesis and cancer cell proliferation. *Proc. Natl Acad. Sci. USA* **103**, 14519–14524 (2006).
7. Kishimoto, K. et al. Hypoxia-induced up-regulation of angiogenin, besides VEGF, is related to progression of oral cancer. *Oral Oncol.* **48**, 1120–1127 (2012).
8. Greenway, M. et al. ANG mutations segregate with familial and 'sporadic' amyotrophic lateral sclerosis. *Nat. Genet.* **38**, 411–413 (2006).
9. Aparicio-Erriu, I. & Prehn, J. Molecular mechanisms in amyotrophic lateral sclerosis: the role of angiogenin, a secreted RNase. *Front. Neurosci.* **6**, 167 (2012).
10. Prehn, J. H. M. & Jirström, E. Angiogenin and tRNA fragments in Parkinson's disease and neurodegeneration. *Acta Pharmacol. Sin.* **41**, 442–446 (2020).
11. Yamasaki, S., Ivanov, P., Hu, G.-F. & Anderson, P. Angiogenin cleaves tRNA and promotes stress-induced translational repression. *J. Cell Biol.* **185**, 35–42 (2009).
12. Ivanov, P., Emara, M. M., Villen, J., Gygi, S. P. & Anderson, P. Angiogenin-induced tRNA fragments inhibit translation initiation. *Mol. Cell* **43**, 613–623 (2011).
13. Fu, H. et al. Stress induces tRNA cleavage by angiogenin in mammalian cells. *FEBS Lett.* **583**, 437–442 (2009).
14. Saxena, S. K., Rybak, S. M., Davey, R. T., Youle, R. J. & Ackerman, E. J. Angiogenin is a cytotoxic, tRNA-specific ribonuclease in the RNase A superfamily. *J. Biol. Chem.* **267**, 21982–21986 (1992).
15. Emara, M. M. et al. Angiogenin-induced tRNA-derived stress-induced RNAs promote stress-induced stress granule assembly. *J. Biol. Chem.* **285**, 10959–10968 (2010).
16. Acharya, K. R., Shapiro, R., Allen, S. C., Riordan, J. F. & Vallee, B. L. Crystal structure of human angiogenin reveals the structural basis for its functional divergence from ribonuclease. *Proc. Natl Acad. Sci. USA* **91**, 2915–2919 (1994).
17. Harper, J. W. & Vallee, B. L. Mutagenesis of aspartic acid-116 enhances the ribonucleolytic activity and angiogenic potency of angiogenin. *Proc. Natl Acad. Sci. USA* **85**, 7139–7143 (1988).
18. Russo, N., Nobile, V., Di Donato, A., Riordan, J. F. & Vallee, B. L. The C-terminal region of human angiogenin has a dual role in enzymatic activity. *Proc. Natl Acad. Sci. USA* **93**, 3243–3247 (1996).
19. Russo, N., Shapiro, R., Acharya, K. R., Riordan, J. F. & Vallee, B. L. Role of glutamine-117 in the ribonucleolytic activity of human angiogenin. *Proc. Natl Acad. Sci. USA* **91**, 2920–2924 (1994).
20. Akiyama, Y., Tomioka, Y., Abe, T., Anderson, P. & Ivanov, P. In lysate RNA digestion provides insights into the angiogenin's specificity towards transfer RNAs. *RNA Biol.* **18**, 2546–2555 (2021).
21. Thomas, S. P., Hoang, T. T., Ressler, V. T. & Raines, R. T. Human angiogenin is a potent cytotoxin in the absence of ribonuclease inhibitor. *RNA* **24**, 1018–1027 (2018).
22. Jardine, A. M. et al. Cleavage of 3',5'-pyrophosphate-linked dinucleotides by ribonuclease A and angiogenin. *Biochemistry* **40**, 10262–10272 (2001).
23. Leonidas, D. D. et al. Refined crystal structures of native human angiogenin and two active site variants: implications for the unique functional properties of an enzyme involved in neovascularisation during tumour growth. *J. Mol. Biol.* **285**, 1209–1233 (1999).
24. Wu, C. C.-C., Zinshteyn, B., Wehner, K. A. & Green, R. High-resolution ribosome profiling defines discrete ribosome elongation states and translational regulation during cellular stress. *Mol. Cell* **73**, 959–970 (2019).
25. Buschauer, R. et al. The Ccr4-not complex monitors the translating ribosome for codon optimality. *Science* **368**, eaay6912 (2020).
26. Ikeuchi, K. et al. Collided ribosomes form a unique structural interface to induce Hel2-driven quality control pathways. *EMBO J.* **38**, e100276 (2019).
27. Yan, L. L. & Zaher, H. S. Ribosome quality control antagonizes the activation of the integrated stress response on colliding ribosomes. *Mol. Cell* **81**, 614–628 (2021).
28. Wlodawer, A., Borkakoti, N., Moss, D. S. & Howlin, B. Comparison of two independently refined models of ribonuclease-A. *Acta Crystallogr. B* **42**, 379–387 (1986).
29. Leonidas, D. D., Shapiro, R., Subbarao, G. V., Russo, A. & Acharya, K. R. Crystallographic studies on the role of the C-terminal segment of human angiogenin in defining enzymatic potency. *Biochemistry* **41**, 2552–2562 (2002).
30. Shapiro, R. Structural features that determine the enzymatic potency and specificity of human angiogenin: threonine-80 and residues 58–70 and 116–123. *Biochemistry* **37**, 6847–6856 (1998).
31. Su, Z., Kuscu, C., Malik, A., Shibata, E. & Dutta, A. Angiogenin generates specific stress-induced tRNA halves and is not involved in tRF-3–mediated gene silencing. *J. Biol. Chem.* **294**, 16930–16941 (2019).
32. St Clair, D. K., Rybak, S. M., Riordan, J. F. & Vallee, B. L. Angiogenin abolishes cell-free protein synthesis by specific ribonucleolytic inactivation of ribosomes. *Proc. Natl Acad. Sci. USA* **84**, 8330–8334 (1987).
33. Akiyama, Y. et al. Selective cleavage at CCA ends and anticodon loops of tRNAs by stress-induced RNases. *Front. Mol. Biosci.* **9**, 791094 (2022).
34. Cristodero, M. & Polacek, N. The multifaceted regulatory potential of tRNA-derived fragments. *Non-coding RNA Invest.* https://doi.org/10.21037/ncri.2017.08.07 (2017).
35. Blanco, S. et al. Stem cell function and stress response are controlled by protein synthesis. *Nature* **534**, 335–340 (2016).
36. Skorupa, A. et al. Motoneurons secrete angiogenin to induce RNA cleavage in astroglia. *J. Neurosci.* **32**, 5024–5038 (2012).
37. Pizzo, E. et al. Ribonuclease/angiogenin inhibitor 1 regulates stress-induced subcellular localization of angiogenin to control growth and survival. *J. Cell Sci.* **126**, 4308–4319 (2013).
38. Saikia, M. et al. Genome-wide identification and quantitative analysis of cleaved tRNA fragments induced by cellular stress. *J. Biol. Chem.* **287**, 42708–42725 (2012).
39. Papageorgiou, A. C., Shapiro, R. & Acharya, K. R. Molecular recognition of human angiogenin by placental ribonuclease inhibitor-an X-ray crystallographic study at 2.0 A resolution. *EMBO J.* **16**, 5162–5177 (1997).
40. Berthelot, F., Bogdanovsky, D., Schapira, G. & Gros, F. Interchangeability of factors and tRNA's in bacterial and eukaryotic translation initiation systems. *Mol. Cell. Biochem.* **1**, 63–72 (1973).
41. Chen, J., Sawyer, N. & Regan, L. Protein–protein interactions: general trends in the relationship between binding affinity and interfacial buried surface area. *Protein Sci.* **22**, 510–515 (2013).
42. Hallahan, T. W., Shapiro, R. & Vallee, B. L. Dual site model for the organogenic activity of angiogenin. *Proc. Natl Acad. Sci. USA* **88**, 2222–2226 (1991).
43. Moroianu, J. & Riordan, J. F. Identification of the nucleolar targeting signal of human angiogenin. *Biochem. Biophys. Res. Commun.* **203**, 1765–1772 (1994).
44. Bradshaw, W. J. et al. Structural insights into human angiogenin variants implicated in Parkinson's disease and amyotrophic lateral sclerosis. *Sci. Rep.* **7**, 41996 (2017).
45. Thiyagarajan, N., Ferguson, R., Subramanian, V. & Acharya, K. R. Structural and molecular insights into the mechanism of action of human angiogenin-ALS variants in neurons. *Nat. Commun.* **3**, 1121 (2012).
46. Bowen, A. M. et al. Ribosomal protein uS19 mutants reveal its role in coordinating ribosome structure and function. *Translation* **3**, e1117703 (2015).
47. Lawson, M. R. et al. Mechanisms that ensure speed and fidelity in eukaryotic translation termination. *Science* **373**, 876–882 (2021).
48. Gromadski, K. B. et al. Kinetics of the Interactions between yeast elongation factors 1 A and 1Bα, guanine nucleotides, and aminoacyl-tRNA. *J. Biol. Chem.* **282**, 35629–35637 (2007).
49. Shapiro, R. & Vallee, B. L. Site-directed mutagenesis of histidine-13 and histidine-114 of human angiogenin. Alanine derivatives inhibit angiogenin-induced angiogenesis. *Biochemistry* **28**, 7401–7408 (1989).
50. Kirby, J. et al. Lack of unique neuropathology in amyotrophic lateral sclerosis associated with p.K54E angiogenin (ANG) mutation. *Neuropathol. Appl. Neurobiol.* **39**, 562–571 (2013).
51. Shao, S. et al. Decoding mammalian ribosome-mRNA states by translational GTPase complexes. *Cell* **167**, 1229–1240 (2016).
52. Rybak, S. M. & Vallee, B. L. Base cleavage specificity of angiogenin with *Saccharomyces cerevisiae* and *Escherichia coli* 5S RNAs. *Biochemistry* **27**, 2288–2294 (1988).
53. Loveland, A. B., Demo, G. & Korostelev, A. A. Cryo-EM of elongating ribosome with EF-Tu•GTP elucidates tRNA proofreading. *Nature* **584**, 640–645 (2020).
54. Blázquez, M., Fominaya, J. M. & Hofsteenge, J. Oxidation of sulfhydryl groups of ribonuclease inhibitor in epithelial cells is sufficient for its intracellular degradation. *J. Biol. Chem.* **271**, 18638–18642 (1996).
55. Czech, A., Wende, S., Mörl, M., Pan, T. & Ignatova, Z. Reversible and rapid transfer-RNA deactivation as a mechanism of translational repression in stress. *PLoS Genet.* **9**, e1003767 (2013).
56. Costa, B. et al. Nicked tRNAs are stable reservoirs of tRNA halves in cells and biofluids. *Proc. Natl Acad. Sci. USA* **120**, e2216330120 (2023).
57. Chen, X. & Wolin, S. L. Transfer RNA halves are found as nicked tRNAs in cells: evidence that nicked tRNAs regulate expression of an RNA repair operon. *RNA* **29**, 620–629 (2023).
58. Akiyama, Y. et al. RTCB complex regulates stress-induced tRNA cleavage. *Int. J. Mol. Sci.* **23**, 13100 (2022).
59. Drino, A. et al. Identification of RNA helicases with unwinding activity on angiogenin-processed tRNAs. *Nucleic Acids Res.* **51**, 1326–1352 (2023).
60. Saikia, M. et al. Angiogenin-cleaved tRNA halves interact with cytochrome c, protecting cells from apoptosis during osmotic stress. *Mol. Cell. Biol.* **34**, 2450–2463 (2014).
61. Chatzileontiadou, D. S. M. et al. The ammonium sulfate inhibition of human angiogenin. *FEBS Lett.* **590**, 3005–3018 (2016).

Methods

Sequence alignment

Sequences of human RNase I (UniProt: P07998) and angiogenin (UniProt: P03950) were trimmed of their signal sequences, then aligned using ClustalOmega in the EMBL-EBI web app[62,63]. Angiogenin numbering throughout is for the 123 amino acid human protein, excluding the 24 amino acid signal peptide as in ref. 64.

Preparation of angiogenin

Recombinant human angiogenin (265-AN/CF) was purchased from R&D Systems, a Bio-Techne Company. The lyophilized stock was resuspended as recommended by the manufacturer in phosphate-buffered saline at 1 mg ml^{-1} or 0.1 mg ml^{-1}. The molar concentrations were derived from absorbance at 280 nm (A_{280}) measurements using the calculated extinction coefficient from https://web.expasy.org/protparam/. Aliquots were flash-frozen in liquid nitrogen and stored at −80 °C. Three independent lots were used in biochemical and cryo-EM experiments, and gave similar results (DK0420031, DK0421061, DK0418081).

Soluble WT and H13A angiogenin were also recombinantly produced using periplasmic expression with a cleavable OmpA signal sequence, almost as previously described[65]. A pET11b vector encoding OmpA signal sequence in frame with the 123 amino acid human angiogenin sequence (codon optimized for *E. coli*) was produced by Genscript. The H13A point mutation was introduced using the Q5 Site-Directed Mutagenesis Kit (New England Bio Labs) and was sequence verified by Sanger sequencing (Azenta Life Sciences). The plasmids were transformed into chemically competent BLR (DE3) cells (EMD Millipore), cultured and purified as described previously[65]. While the yields of angiogenin were low (30 µg per 100 ml culture), both the WT and H13A mutant yielded bands on SDS–PAGE gels and western blots like the product from R&D Systems, and the WT protein cleaved tRNA in an 80S-stimulated manner (Extended Data Fig. 3e–h). The concentration of WT angiogenin was assessed using the molar extinction coefficient and confirmed by Coomassie-stained gel against the R&D Systems angiogenin. The concentration of angiogenin(H13A) was titrated to match the R&D Systems angiogenin using Coomassie gel staining and western blotting due to low yield and the presence of a contaminant. The soluble angiogenin(H13A) was used for the cryo-EM dataset and revealed the fold of angiogenin, the H13A site mutation (Extended Data Fig. 6c) and no extra density at the N terminus of angiogenin for the OmpA signal sequence.

Refolded WT, H13A and K54E angiogenin were also recombinantly produced using overexpression to inclusion bodies, solubilization and refolding, and purification using modification of previously described protocols[66,67]. The pET11b-proOmpA-Angiogenin vector described above was altered using the Q5 Site-Directed Mutagenesis Kit (New England Bio Labs) to remove the OmpA signal sequence, leaving a start codon followed by the 123 nucleotide sequence of angiogenin without any tags. Plasmids with H13A and K54E mutations were also generated using the same mutagenesis kit and all were verified by Sanger sequencing (Azenta Life Sciences). The plasmids were transformed into chemically competent BLR (DE3) cells (EMD Millipore); the cells were cultured, induced and collected; and the inclusion bodies were purified and protein refolded as described previously[66]. The refolded proteins were purified using CM-sepharose and heparin chromatography similarly to the soluble angiogenin preparation described above. The proteins were concentrated using 10,000 MWCO Amicon filters (MilliporeSigma), exchanged to a buffer compatible with mammalian translation assays (20 mM Tris-Acetate pH 7.0, 100 mM KOAc) and aliquots were flash-frozen in liquid nitrogen for future use. The yields of angiogenin were more than 10 times higher using the refolding protocol (>300 µg per 100 ml culture), and bands on SDS–PAGE gels were at the same position as the product from R&D Systems and the soluble angiogenin preparations. The concentration of refolded angiogenins was assessed using the molar extinction coefficient at 280 nm.

Preparation of tRNA^{Ala}

Yeast tRNA^{Ala} (anticodon AGC) was produced by in vitro transcription as follows: the gene encoding tRNA^{Ala} (anticodon AGC) and preceded by the T7 RNA polymerase promoter was synthesized and cloned into pUC57 between the EcoRI and BamHI sites by GeneScript. The T7 promoter and tRNA^{Ala}-encoding region was then PCR amplified using primers (Integrated DNA Technologies) encoding the T7 promoter (5′-GAATTCTAATACGACTCACTATAGGGCGTG) and the 3′ end of the tRNA including the non-templated CCA of mature tRNA (5′-TGGTGGACGAGTCCGG-3′). The PCR product was used as a template for run-off in vitro transcription using T7 polymerase as previously described[68]. The in vitro transcribed tRNA (IVT tRNA) was folded by heating to 65 °C and slowly cooling to room temperature for 30 min in refolding buffer (20 mM KOAc pH 7.5, 20 mM $MgCl_2$). tRNA purity was confirmed by PAGE and concentration was determined using the absorbance at 260 nm (1,800 pmol ml^{-1} per A_{260} (1 cm)). The stock solution was stored at −80 °C.

tRNA^{Ala} was charged with alanine using yeast S100 extract from the protease-deficient strain BJ2168. To prepare S100 extract, 6 l of BJ2168 cells was grown until an optical density at 600 nm (OD_{600}) of 1.5 in YPD, pelleted and then flash-frozen. The frozen cells were ground in a ball-mill grinder (Retsch) and resuspended in 20 ml of S100 lysis buffer (10 mM $KHPO_4$ pH 7.5, 1× Mini protease inhibitor cocktail tablet (Roche)) for 1 h. This and all of the subsequent steps took place at 4 °C. The lysate was clarified by centrifugation at 20,000*g* for 0.5 h (Beckman Coulter). The ribosomes were pelleted from the clarified lysate by ultracentrifugation in a Ti-70 rotor at 100,000*g* for 3 h. The top 80% of the post-ribosomal supernatant was collected and incubated with DEAE cellulose resin (2.5 g dry weight before washing; Sigma-Aldrich) prewashed with S100 lysis buffer for 0.5 h. The resin was recovered and washed twice with 10 column volumes (CV) of S100 lysis buffer on a gravity-flow column (Bio-Rad Laboratories). The S100 extract was eluted from DEAE resin with 5 ml of S100 elution buffer (250 mM $KHPO_4$ (pH 6.5), 1× Mini protease inhibitor cocktail tablet (Roche)) and aliquoted and flash-frozen in liquid nitrogen. Folded IVT tRNA^{Ala} (77 µM) was incubated with 1 mM L-alanine and 20% *Saccharomyces cerevisiae* S100 extract in 1× charging buffer (50 mM HEPES-KOH pH 7.5, 10 mM KCl, 50 mM $MgCl_2$, 30 µM $ZnCl_2$, 12 mM ATP, 1 mM DTT) at 25 °C for 20 h. The charged tRNA (Ala-tRNA^{Ala}) was phenol extracted twice, chloroform:isoamyl (24:1) extracted twice, and then ethanol precipitated in the presence of NaOAc pH 5.2. The resulting pellet was washed with cold, 70% ethanol. The precipitated Ala-tRNA^{Ala} was resuspended in 2 mM NaOAc pH 5.2. Aminoacylated-tRNA was further separated from excess ATP by passing through a Sephadex G-25 column in 2 mM NaOAc pH 5.2. The concentration of sample was determined using the absorbance at 260 nm (1,800 pmol ml^{-1} per A_{260} (1 cm) unit) and the extent of aminoacylation was determined by acidic PAGE[69] and was >90%. The Ala-tRNA^{Ala} solution was stored at −80 °C before use.

Purification of eEF1A

Yeast eEF1A was purified from *S. cerevisiae* BJ2168 with some modification[70]. Yeast eEF1 is >80% sequence identical to rabbit eEF1A and can fully substitute the function of mammalian eEF1A in a mammalian translation system[71]. To obtain endogenous eEF1A, 6.5 ml of flash-frozen BJ2168 cells were ground in a liquid-nitrogen-cooled ball mill (Retsch) and were resuspended in 10 ml of buffer A (20 mM Tris-HCl pH 7.5, 0.1 mM EDTA, 25% glycerol, 100 mM KCl, 1 mM DTT, 1× Mini protease inhibitor cocktail tablet (Roche), 2 mM PMSF (Sigma-Aldrich)) and stirred for 1 h at 4 °C. The lysate was clarified by centrifugation at 31,745*g* in a JA20 rotor (Beckman Coulter) for 15 min at 4 °C and the soluble portion was retained. This clarification step was repeated twice. The clarified lysate was loaded onto a pre-washed/pre-equilibrated CM

Sepharose HiTrap column (5 ml, GE Healthcare) on the Äkta explorer FPLC (GE Healthcare) system. The column was washed with 12 CV of buffer A and then eluted with a 0–100% gradient of buffer B (20 mM Tris pH 7.5, 0.1 mM EDTA, 25% glycerol, 1 M KCl, 1 mM DTT, 1× Mini protease inhibitor cocktail tablet (Roche) and 2 mM PMSF) over 10 CV. Elution profile and SDS–PAGE analysis revealed that eEF1A eluted at 23.4% gradient of buffer B. The peak fractions were diluted to a final KCl concentration of 50 mM with buffer C (20 mM HEPES pH 7.5, 0.1 mM EDTA, 25% glycerol, 1 mM DTT, 1× Mini protease inhibitor cocktail tablet (Roche)) and filtered (0.2 µm pore size). The solution was then injected onto a prewashed SP Sepharose HiTrap column (5 ml, GE Healthcare). The column was washed with 20 CV of buffer D (20 mM HEPES-KOH pH 7.5, 0.1 mM EDTA, 25% glycerol, 50 mM KCl, 1 mM DTT, 1× Mini protease inhibitor cocktail tablet (Roche)) and was then eluted through a stepwise gradient with buffer E (20 mM HEPES pH 7.5, 0.1 mM EDTA, 25% glycerol, 1 M KCl, 1 mM DTT, 1× Mini protease inhibitor cocktail tablet (Roche)) as follows: 15% buffer E for 5 CV, 30% buffer E for 5 CV, 50% buffer E for 5 CV and 100% buffer E for 5 CV. The eEF1A fraction eluted at ~30% buffer E and was exchanged to buffer F (20 mM HEPES pH 7.5, 0.1 mM EDTA, 25% glycerol, 100 mM KCl, 2 mM $MgCl_2$, 1 mM DTT, 1× Mini protease inhibitor cocktail tablet (Roche)) using an Amicon Ultra centrifugal filter unit with an MWCO of 10 kDa (MilliporeSigma). The protein was further purified by gel-filtration chromatography on the Superdex 75 16/60 column with buffer F. The eEF1A-containing peak was identified by 12% SDS–PAGE, pooled, concentrated and stored at −20 °C.

Purification of ribosomal subunits

Ribosomal subunits were purified from nuclease-untreated RRL (Green Hectares) as described previously[72] except that 40S and 60S subunits were purified twice over a sucrose gradient and the middle ~10% of each peak was taken to reduce trace 40S, 60S and 80S contaminants in each subunit preparation. These doubly purified 40S and 60S subunits were used to test the activity of angiogenin dependent on 40S or 60S subunits and various mRNAs (Extended Data Fig. 4). Double purification of 60S subunits reduced the apparent activation of angiogenin as compared to single sucrose-gradient purification of 60S subunits, suggesting that fractional contamination by 40S/80S ribosome complexes results in apparent trace activation by 60S subunits.

Purification of total rabbit tRNA

Total rabbit tRNA was purified from the ribosome-depleted supernatant of RRL leftover from the first centrifugation step of ribosomal subunit preparation described above and ref. 72. In total, 200 µl of RRL supernatant was purified per miRNAeasy column (Qiagen) according to the manufacturer's recommended protocol and eluting in 14 µl. High-molecular-mass species (rRNA or contaminating DNA) were further removed by diluting into 50 µl in 0.3 M NaOAc then adding 0.54 volumes of isopropanol, incubating for 5 min at room temperature, then precipitating in a room temperature microfuge at 16,000*g* for 5 min. The supernatant was retained and the tRNA was precipitated by supplementing isopropanol to 50%, incubating 10 min at room temperature, then precipitating in a room temperature microfuge at 14,000*g* for 15 min. The pellet was washed once with 80% ethanol, dried and resuspended in 25 µl of water and its concentration was determined based on its absorbance at 260 nm. The total tRNA was supplemented with 1×10 buffer (50 mM Tris-Acetate pH 7.0, 100 mM KOAc, 10 mM $Mg(OAc)_2$) and was diluted to 0.8 OD ml^{-1}. The total tRNA was refolded by heating to 90 °C for 1 min then cooling to room temperature in a Thermomixer R (Eppendorf). The solution was used immediately for cleavage assays or stored for future use at −80 °C.

Translation in RRL

RRL were used to study the inhibition of translation by angiogenin. We monitored translation of an mRNA encoding nanoluciferase[73] in micrococcal-nuclease-treated RRL (Promega). In these experiments, 70% (final concentration) nuclease-treated RRL (Promega) was supplemented with 0.02 mM amino acids (Promega), 1% Nano-Glo nanoluciferase substrate (Promega) and the indicated concentration of angiogenin or matching protein buffer with or without 0.8 U $µl^{-1}$ rRNasin (Promega) for 15 min at 30 °C, similarly to the 15 min angiogenin preincubation described previously[14]. Next, 10 ng $µl^{-1}$ (final concentration) 6×His-Nanoluciferase mRNA flanked with the 5′- and 3′-UTR from rabbit β-globin[74] was added, forming a 10 µl reaction mixture, and translation was followed over time by measuring the luminescence of Nanoluciferase using an Infinite m1000 PRO or a Spark microplate reader (Tecan) for 15 min at 30 °C. The slope of the luminescence signal between 200 to 300 s (initial burst of nanoluciferase synthesis for an uninhibited reaction) was measured in Prism 8 (GraphPad Software) for each condition across the indicated number of experiments and is plotted as the rate of translation (RLU s^{-1}) in Fig. 1a and Extended Data Fig. 3i,j. For Fig. 2k and Extended Data Fig. 3c, the maximum rate of translation (RLU s^{-1}) was calculated in Prism 9 (GraphPad Software) by taking the maximum value of the first derivative of the RLU curve without smoothing. The IC_{50} values for translation inhibition by WT, H13A or K54E angiogenin (Fig. 2k) were obtained by fitting the maximum rate of translation versus protein concentration in Prism 9 (GraphPad Software), using the [Inhibitor] versus response (three parameters) model but constraining the bottom parameter to equal zero and asking for symmetrical confidence intervals, reporting IC_{50} ± s.e. In Fig. 1b, the 9 µl reaction mixtures containing RRL and angiogenin before mRNA addition were stopped at 15 min by 5 volumes of 8 M urea loading buffer (8 M urea, 2 mM Tris-HCl pH 8, 20 mM EDTA). The reactions were heated at 65 °C for 5 min, centrifuged, vortexed and 5 µl was loaded onto a 15% pre-cast Novex Urea-TBE gel (Thermo Fisher Scientific) and run at 180 V for 60 min alongside Small RNA Marker (Ab Nova). The gels were stained in 1× TBE with 1:20,000 SYBR Gold nucleic acid stain (Thermo Fisher Scientific) for 30 min and imaged on a ChemiDoc MP system (Bio-Rad Laboratories) using the UV light mode for SYBR Gold.

Association of angiogenin with ribosome

Separation of RRL translation reactions into supernatant and ribosome pellet fractions was performed in RRL left untreated with micrococcal nuclease (Green Hectares), so that it contained endogenous mRNA. Translation reactions (50 µl, containing 50% RRL, 30 µM hemin (Sigma-Aldrich), 75 mM KCl, 0.5 mM $MgCl_2$, 1 mM ATP, 0.2 mM GTP, 2.1 mg ml^{-1} creatine phosphate, 30 µM of L-amino acid mix, 15 mg ml^{-1} yeast tRNA, 6 mM βME, all final concentrations) were assembled adding as the last component (1) buffer, (2) 1 µM of indicated angiogenin or (3) 1 µM angiogenin preincubated for 5 min with 8 U $µl^{-1}$ (final concentrations) rRNasin (Promega). The reactions were performed in a heat block at 37 °C. After 5 min, the reactions were terminated by addition of 100 µl of ice-cold 1×10 buffer (50 mM Tris-Acetate pH 7.0, 100 mM KOAc, 10 mM $Mg(OAc)_2$) with 10 mM βME. The reactions were applied to 15% (w/v) sucrose cushions in 1×10 buffer with 10 mM βME and centrifuged in an TLA-110 rotor in an Optima MAX-TL ultracentrifuge (Beckman Coulter) at 408,800*g* (average) for 1 h at 4 °C. The top third (1 ml) of the sucrose cushion was collected as the supernatant fraction and 2 µl were loaded per lane on the western blot shown in Fig. 1c and Fig. 2j. The ribosome pellet was washed in 1×10 buffer with 10 mM βME and was then resuspended in 40 µl of 1×10 buffer with 10 mM βME using a microstirbar and pipetting. The A_{260} of the ribosome fractions was measured and 10 OD units were loaded per lane on the western blots shown in Fig. 1c and Fig. 2j.

Alternatively, we assessed angiogenin or RNase A (Thermo Fisher Scientific) interactions with ribosomes in the absence of competing translation factors and tRNA. Here, we used the crude ribosomes from RRL purified by a single sucrose cushion pelleting step[72]. We incubated 20 pmol crude ribosomes with 20 pmol of angiogenin or RNase A for 5 min at 37 °C in 100 µl of 1×10 buffer with 10 mM βME. The ribosomes were separated from free proteins on 15% (w/v) sucrose cushions

(as described above for RRL reactions). The top third (1 ml) of the sucrose cushion was collected as the supernatant fraction and 5 µl (1:200) or 40 µl (1:25) was loaded per lane on the western blot shown in Extended Data Fig. 3b. The ribosome pellet was washed in 1×10 buffer with 10 mM βME and was then resuspended in 60 µl Laemmli buffer and 10 µl was loaded onto the western blot shown in Extended Data Fig. 3b.

Western blotting

Samples alongside Precision Plus Protein Dual Colour Standard or Xtra ladder (Bio-Rad Laboratories) were run on 4–20% Mini-Protean TGX Precast Protein gels (Bio-Rad Laboratories) at 120 V for 1 h in 1× Tris-Tricine-SDS running buffer. The gels were transferred onto a PVDF membrane, 0.2 µm pore size (Bio-Rad Laboratories) in 1× Tris-Glycine buffer with 20% methanol. The membranes were blocked in 1× PBS + 0.1% Tween-20 (1× PBST) buffer with 6% Blotto non-fat milk powder (Santa Cruz Biotechnologies). After 4 washes in 1× PBST with shaking for 5 min each, the membranes were incubated with either 1:500–1:1000 mouse anti-angiogenin monoclonal antibody C-1 (sc-74528, Santa Cruz Biotechnologies) or 1:500 mouse anti-ribosomal protein s5 monoclonal antibody (A-8) (sc-390935, Santa Cruz Biotechnologies) in 1× PBST with 6% milk powder for 1 h at room temperature or overnight at 4 °C. After four washes with shaking in 1× PBST for 5 min each, the membranes were incubated with 1:10,000 goat anti-mouse IgG (H+L)-HRP conjugate (62–6520, Thermo Fisher Scientific) secondary antibodies in 1× PBST + 6% milk powder for 30 min. After four washes in 1× PBST for 5 min each, the blot was developed using SuperSignal West Femto Maximum Sensitivity Substrate (Thermo Fisher Scientific) and imaged on the ChemiDoc MP system (Bio-Rad Laboratories) using the chemiluminescence setting for western imaging and colorimetric setting to capture the ladder. For anti-RNase A blotting, procedures were amended to block with 1× PBST with 0.1 mg ml^{-1} BSA and detected with 1:1,000 rabbit anti-bovine pancreatic RNase A polyclonal antibody-peroxidase conjugated (200-4388S, Rockland Immunochemicals). Full scans of gel images are available in Supplementary Fig. 1.

Cryo-EM sample preparation

For visualizing 80S–angiogenin in RRL, translation reactions (20 µl, containing 33% RRL (Green Hectares), 60 µM hemin (Sigma-Aldrich), 75 mM KCl, 0.5 mM $MgCl_2$, 1 mM ATP, 0.2 mM GTP, 2.1 mg ml^{-1} creatine phosphate, 30 µM of L-amino acid mix, 6 mM βME, 0.4% Nano-Glo endurazine (Promega), all final concentrations) were supplemented with either water or 1 µM angiogenin (in 20 mM Tris-HCl pH 7.5 + 50 mM NaCl; final concentration) (R&D Systems), then, 5 min later, with 2.5 ng $µl^{-1}$ 6×His-Nanoluciferase mRNA (final concentration). After incubation for 10 min at 37 °C, the RRL was placed on ice and used for cryo-plunging as described below. The remaining 10 µl of each reaction was flash-frozen and later thawed and applied to a 384-well plate for reading in the Spark microplate reader (Tecan). The luminescence signal from the water-supplemented sample showed translation occurred (293,050 RLU) while with 1 µM angiogenin luminescence was at background levels (54 RLU).

For in vitro assembled complexes, *Oryctolagus cuniculus* (European rabbit) 80S ribosomes with angiogenin were prepared with or without a ternary complex of eEF1A, Ala-$tRNA^{Ala}$ and GDPCP. Rabbit 60S subunits (2 µM) were pre-incubated for 5 min at 30 °C in 1×10 buffer (20 mM Tris-acetate (pH 7.0), 100 mM KOAc, 10 mM $Mg(OAc)_2$). Meanwhile, 40S subunits were preincubated with a leaderless mRNA encoding the start codon in the P-site and the UUC Phe codon in the A-site (CCAC-AUG-**UUC**-CCC-CCC-CCC-CCC-CCC-CCC, Integrated DNA Technologies) for 5 min at 30 °C in the same buffer. *E. coli* $tRNA^{fMet}$ (Chemical Block) was added to 40S such that final concentrations were 1.2 µM 40S, 40 µM mRNA and 2.4 µM $tRNA^{fMet}$. The 40S and 60S reactions were mixed 1:1 and incubated for 5 min at 30 °C to form the 80S ribosome with $tRNA^{fMet}$ and AUG codon in the P site. Next, either 4 µM WT angiogenin or ~400 nM angiogenin(H13A) (final concentrations) was added while diluting the 80S complex by half in 1×10 buffer and incubated for 5 min at 30 °C. The resulting 80S–angiogenin complex (containing 0.5 µM 60S, 0.3 µM 40S, 10 µM mRNA, 0.6 µM $tRNA^{fMet}$ and 4 µM angiogenin or 400 nM angiogenin(H13A)) was flash-frozen in liquid nitrogen, stored at −80 °C and was thawed immediately before grid plunging. A ternary complex of eEF1A, Ala-$tRNA^{Ala}$ and GDPCP was assembled in 1×10 buffer by preincubation of eEF1A and GDPCP (Jena Bioscience) for 5 min at 30 °C followed by addition of Ala-$tRNA^{Ala}$ for 1 min at 30 °C. The resulting ternary complex reaction (containing 24 µM eEF1A, 4 µM Ala-$tRNA^{Ala}$ and 1 mM GDPCP) was also flash-frozen in liquid nitrogen and was stored at −80 °C.

For angiogenin in RRL, 80S–angiogenin complex, 80S–angiogenin(WT)–ternary complex and 80S–angiogenin(H13A)–ternary complex, Quantifoil R2/1 holey-carbon grids coated with a thin layer of carbon (Electron Microscopy Service) were glow discharged with 20 mA current with negative polarity for 30 s (with ternary complex or RRL) or 60 s (without ternary complex) in a PELCO easiGlow glow discharge unit. The Vitrobot Mark IV (Thermo Fisher Scientific) was pre-equilibrated to 5 °C and 95% relative humidity and the blot force was set to 10. For angiogenin-supplemented RRL reactions, 4 µl of lysate was applied to the grid, incubated for 10 s, blotted and then plunged into liquid-nitrogen-cooled liquid ethane. For the 80S–angiogenin complex, a similar procedure was used, but only 2.5 µl of the 80S–angiogenin reaction was applied to the grid. For the 80S–angiogenin(WT)–ternary complex, 1.5 µl of 80S–angiogenin was mixed with 1.5 µl of ternary complex in an ice-cold tube with ice-chilled tips and was applied as quickly as possible to the grid or with a 30 s delay. The solution was incubated on the grid for 10 s, blotted for 4 s and then plunged into liquid-nitrogen-cooled liquid ethane. The total elapsed time from mixing 80S–angiogenin with ternary complex to cryo-plunging was either 25 s or 60 s. 15% TBE-urea gel electrophoresis analysis of a time course of the same reactions (80S–angiogenin and ternary complex) showed that cleavage of Ala-$tRNA^{Ala}$ nearly saturates within 25 s (Extended Data Fig. 5e); thus, the 25 s timepoint was chosen for cryo-EM analysis. For the 80S–angiogenin(H13A)–ternary complex reaction, 1.5 µl of 80S–angiogenin(H13A) was mixed with 1.5 µl of ternary complex and was incubated for 5 min at 30 °C. Then, 3 µl of 80S–angiogenin(H13A)–ternary complex reaction was applied to the grid for 10 s, blotted for 4 s and then cryo-plunged. Gel analysis showed no increase in tRNA fragments in these H13A samples (Extended Data Fig. 5f).

EM analysis

Data for 80S–angiogenin and 80S–angiogenin(WT)–ternary complex were collected on the Talos electron microscope (Thermo Fisher Scientific) operating at 200 kV and equipped with a K3 direct electron detector (Gatan) targeting 0.5 µm to 1.8 µm underfocus. Data collection was automated using SerialEM[75] using beam tilt to collect multiple videos (for example, five videos per hole at four holes) at each stage position[76]. The 80S–angiogenin dataset had 1,015 videos, at 20 frames per video at 1.1 $e^- Å^{-2}$ per frame for a total dose of 29.6 $e^- Å^{-2}$ on the sample and yielding 107,236 particles. The 80S–angiogenin–ternary complex dataset had a total of 20 frames per video, with 1.55 $e^- Å^{-2}$ per frame for a total dose of 30.9 $e^- Å^{-2}$ on the sample, comprising 5,044 videos yielding 273,774 particles. The videos were aligned during data collection using IMOD[77] to decompress frames, apply the gain reference, and correct for image drift and particle damage and bin the super-resolution pixel by 2 to 0.87 Å in the final image sums.

Data for the angiogenin-supplemented RRL and 80S–angiogenin (H13A)–ternary complex reactions were collected on the Krios electron microscope (Thermo Fisher Scientific) operating at 300 kV and equipped with a Gatan Image Filter (slit width, 20 eV) and a K3 direct electron detector (Gatan) and a targeting 0.5 µm to 1.5 µm underfocus. Data collection was automated using SerialEM[75] using beam tilt to collect multiple videos (4–6 videos per hole at nine holes) at each stage position[76]. The angiogenin-supplemented RRL dataset had 10,084

videos, at 18 frames per video at 1.7 e^{-} Å^{-2} per frame for a total dose of 30 e^{-} Å^{-2} on the sample. The videos were aligned during data collection using IMOD[77] to decompress frames, apply the gain reference, and to correct for image drift and bin the super-resolution pixel by 2 to 0.83 Å in the final image sums. The 80S–angiogenin(H13A)–ternary complex dataset had a total of 11,630 videos, with 18 frames per video, with 1.7 e^{-} Å^{-2} per frame for a total dose of 30 e^{-} Å^{-2} on the sample, yielding 451,181 particles. The hardware-binned videos were aligned during data collection using IMOD[77] to decompress frames, apply the gain reference and correct for image drift in the final image sums.

Cryo-EM data classification and refinement

CTF determination, reference-free particle picking and stack creation were performed in cisTEM[78]. Particle alignment and refinement were performed in Frealign v.9.11 and cisTEM[78,79]. The box size for all datasets was 608 × 608 × 608. To speed up processing, binned image stacks (for example, 8×, 4× or 2×) were prepared using the resample.exe part of the Frealign v.9.11 distribution. The initial model for particle alignment of 80S maps was EMD-4729 (ref. 80), which was downsampled to match the 8×-binned stack and low-pass filtered to 30 Å using EMAN2[81]. Two rounds of mode 3 search alignment to 30 then 20 Å were performed using the 8×-binned stack. Next, rounds of mode 1 refinement were run with the 4×-binned and eventually the 2×-binned stack as we gradually added resolution shells to 8 Å.

For the reconstituted 80S–angiogenin dataset, focused 3D maximum-likelihood classification into 6 classes (using the high-resolution limit of 12 Å and the 4×-binned stack, 30 rounds) with a 45 Å spherical mask covering the A site of the ribosome (x, y, z = 225.405, 278.628, 242.574) resolved different ribosome states, including two angiogenin-bound classes. The particles from these two classes were extracted using merge_classes.exe, setting a threshold of class occupancy of 0.50 and score of 0. The resulting stack of 45,850 particles was independently refined starting from the EMD-4729 starting model until the high-resolution limit of 5 Å and was further improved by one round of per-particle CTF refinement to yield the final map at 3.04 Å resolution.

For the 80S–angiogenin–ternary complex dataset, focused 3D maximum-likelihood classification into 8 classes (using the high-resolution limit of 15 Å and the 8×-binned stack, 50 rounds) with a 50 Å spherical mask covering the A site and the GTPase-activating centre of the ribosome (x, y, z = 225.756, 296.851, 200.364) resolved different ribosome states (Extended Data Fig. 5a), including the three 80S–angiogenin classes, one 80S–angiogenin–tRNA^{Ala} state. The three 80S–angiogenin classes were merged yielding a 101,572-particle stack, independently refined and improved with per-particle CTF refinement followed by beam-tilt refinement to yield a map with a resolution of 2.81 Å (the high resolution limit for refinement was 4 Å). The 80S–angiogenin–tRNA^{Ala} particles were extracted and further separated using focused 3D maximum-likelihood classification into 6 classes (using a high-resolution limit of 15 Å and the 8×-binned stack, 100 rounds) using a 60 Å mask around the A-site and GTPase-activating centre and encompassing eEF1A (x, y, z = 253.211, 303.049, 190.051). This classification yielded five 80S–angiogenin–tRNA^{Ala} classes and one 80S–angiogenin–Ala-tRNA^{Ala}–eEF1A–GDPCP state (Extended Data Fig. 5a). The five 80S–angiogenin–tRNA^{Ala} classes were merged, yielding a 17,593-particle stack, independently refined and improved with per-particle CTF refinement followed by beam-tilt refinement to yield a map at 3.09 Å resolution (the high resolution limit for refinement was 5 Å). The 80S–angiogenin–Ala-tRNA^{Ala}–eEF1A–GDPCP particles were independently extracted, yielding a 3,604-particle stack that, once refined and beam-tilt corrected, yielded a map at 3.67 Å resolution (the high resolution limit for refinement was 9 Å). Finally, the particles from the rotated 40S class were extracted yielding a 36,105-particle class that was further separated using focused 3D maximum-likelihood classification into 6 classes (using a high-resolution limit of 15 Å and the 8×-binned stack, 50 rounds) and a 50 Å mask around the head of 40S subunit and encompassing the three tRNA-binding sites (x, y, z = 194.690, 263.751, 232.504). This classification yielded three rotated, hybrid-state classes with either one or two tRNAs (P/E or A/P and P/E) and without angiogenin; two classes with partial subunit rotation (~8.5° 40S body rotation and ~0° head rotation) and with classical-state-like tRNAs in the E/E and P/P sites and angiogenin in the A site; and one non-rotated class with two classical-state tRNAs and weak angiogenin density. Angiogenin density was lower resolution in the partially subunit-rotated classes than in the main maps described above, and angiogenin interacts predominantly with H69.

For the reconstituted 80S–angiogenin(H13A) dataset, focused 3D maximum-likelihood classification into 24 classes (using the high-resolution limit of 16 Å and the 8×-binned stack, 200 rounds) with a 50 Å spherical mask covering the A site of the ribosome (x, y, z = 231.443, 277.244, 193.718) resolved different ribosome states including two angiogenin-bound classes and one class with angiogenin and tRNA (Extended Data Fig. 5c). The particles from the first two classes were extracted using merge_classes.exe, setting a threshold of class occupancy of 0.50 and score of 0. The resulting stack of 17,220 particles was independently refined and improved with per-particle CTF refinement followed by beam-tilt refinement to yield a map at 2.84 Å resolution (the high resolution limit for refinement was 4.75 Å). The particles from the remaining 80S–H13 angiogenin–tRNA^{Ala} were extracted and further separated using focused 3D maximum-likelihood classification into 3 classes (using a high-resolution limit of 15 Å and the 8×-binned stack, 100 rounds) using a 30 Å mask around the tRNA^{Ala} (x, y, z = 230.083, 293.639, 194.267). This classification yielded improved 80S–angiogenin(H13A)–tRNA^{Ala} classes (Extended Data Fig. 5c). The class was extracted yielding a 2,613-particle stack, independently refined to yield a map at 3.88 Å resolution (the high resolution limit used for refinement was 9 Å).

Processing of the angiogenin-supplemented RRL was performed differently compared with for the purified samples because the standard cisTEM/Frealign pipeline did not yield high-resolution maps due to poor particle picking. Other pipelines, including Relion, cryoSPARC and other packages were also tried but did not yield the same diversity of classes as the following method. CTF determination and initial reference-free particle picking were performed in cisTEM, but we resorted to improving cisTEM picking by hand for the subset of ~600 micrographs, which had CTFFIND 4 fit resolution values between 2 and 3.2 Å and, we reasoned, thinner, flatter ice. The improved picks resulted in a 6,216-particle stack that was auto refined in cisTEM[78] using a 60 Å low-passed filtered EMD-4729 (ref. 80) as the initial model, and yielded a 3.31 Å overall map. The aligned parameters and stack were exported from cisTEM to Frealign, where optimal separation of classes was achieved using a focused 3D maximum-likelihood classification into 6 classes (high-resolution limit of 16 Å and the 8×-binned stack, 100 rounds) with a 60 Å mask around the A-site (x, y, z = 219.341, 306.909, 205.780). The two classes with angiogenin bound in the A-site were combined yielding a 1,960-particle stack. This stack was independently aligned and refined to yield a 3.36 Å map (the limit for refinement was 10 Å). The RRL–angiogenin map was also improved by applying a binary mask using standard procedures in EMAN2[81].

Structural model building and refinement

The cryo-EM structure of the $(GR)_{20}$-bound *O. cuniculus* ribosome complex (PDB: 7TOR), omitting $(GR)_{20}$ and P-tRNA, was used as the starting model for structure refinement for all maps. Domains (60S, 40S head with mRNA, 40S body, E-tRNA, L1 stalk and P stalk) of the 80S were rigid-body fitted into each cryo-EM map using Chimera[82]. The P-tRNA structure was modelled from PDB: 5UYM (ref. 53). Angiogenin was modelled from PDB: 5EOP (ref. 61), and was remodelled in Coot (v.0.8.2)[83] to fit the density in the 80S–angiogenin map. Yeast tRNA^{Ala} with the AGC anticodon was modelled in Coot (v.0.8.2), using yeast

tRNA^{Phe} crystal structure as a starting model (PDB: 1EHZ)[84]. The yeast eEF1A starting model was from AlphaFold (https://alphafold.ebi.ac.uk/entry/P02994)[85,86] and the interaction of acceptor arm of tRNA^{Ala} with eEF1A was modelled from the ribosome-bound ternary complex in PDB: 5LZS (ref. 51).

The models were refined using real-space simulated-annealing refinement using RSRef[87,88] against corresponding maps. Refinement parameters, such as the relative weighting of stereochemical restraints and experimental energy term, were optimized to produce the optimal structure stereochemistry, real-space correlation coefficient and *R*-factor, which report on the fit of the model to the map[89]. Harmonic restraints were used for the lower-resolution features of tRNA and eEF1A to maintain secondary structure. The structures were next refined using phenix.real_space_refine (Phenix v.1.14)[90,91] to optimize protein geometry and *B*-factors. The resulting structural models have good stereochemical parameters, characterized by low deviation from ideal bond lengths and angles and agree closely with the corresponding maps as indicated by high correlation coefficients and low real-space *R* factors (Extended Data Table 1). Figures were prepared in Pymol[92] and Chimera[82].

To visualize the dynamics of tRNA and the P-stalk (Fig. 3e), cryo-EM maps from the six-way classification that yielded the 80S–angiogenin–tRNA^{Ala} were low-pass filtered to 6 Å and rigid-body fitted in Chimera[82] using the final 80S–angiogenin–tRNA^{Ala} model (maps and fits are shown in Supplementary Videos 1 and 2). For Fig. 3e, these rigid-fit models were superimposed through the 28S rRNA excluding the flexible P-stalk and L1 stalks, and the differences in tRNA positions at the acceptor arm and tRNA elbow were measured in Pymol.

RRL–angiogenin and 80S–angiogenin(H13A) cryo-EM maps were interpreted by rigid-body fits in Chimera[82] using our three in vitro assembled models or PDB entries as noted in the figure panels.

Unstimulated angiogenin nuclease assay

Nuclease activity of refolded angiogenins against tRNA (Extended Data Fig. 3d) was measured by following the formation of acid soluble fragments similarly to as described previously[3,44]. Yeast tRNA (2 mg ml^{-1}; Sigma-Aldrich) was incubated with 500 nM refolded angiogenin with or without 4 U µl^{-1} of rRNasin (Promega) in 33 mM HEPES-NaOH pH 7, 33 mM NaCl, 0.1 mg ml^{-1} recombinant albumin (New England Bio Labs) for 2 h at 37 °C. The reactions were stopped by addition of trichloroacetic acid to 10%, centrifuged at 16,000*g* and the acid soluble supernatant was collected and then neutralized with 2 volumes of 1 M sodium bicarbonate before measurement of the A_{260} on a the NanoDrop 1000 (Thermo Fisher Scientific) system. The average value of reactions not treated with angiogenin was taken as the background (0% activity) and the average value of the WT reaction was normalized as 100% activity.

Ribosome-stimulated nuclease assays

To ascertain whether angiogenin is activated by ribosome binding, we tested tRNA cleavage by angiogenin under conditions similar to those used for assembling the angiogenin-bound cryo-EM complexes, using the same preparations of ribosomal subunits, various mRNA sequences, preparations of angiogenin and tRNAs, at varied relative concentrations. Materials were maintained and assays were performed under conditions that limited RNase contamination, including use of ultrapure water, RNase-free-rated plastic tubes and tips, limiting dust in the work area, wiping down of pipettes with RNase Away and frequent changing of gloves. Notably, the use of a facemask (KF94, KM) reduced non-specific RNase activity as judged by the appearance of wells having a smear rather than specific bands visible after SYBR Gold staining. After lifting of the local mask mandate, experiments with such contamination increased in frequency. They were discarded and repeated with masking.

To assemble the 80S ribosomal complexes, 60S subunits were diluted to 1 µM in 1×10 buffer (50 mM Tris-Acetate pH 7.0, 100 mM KOAc, 10 mM $Mg(OAc)_2$) with 10 mM βME and the mixture was incubated for 5 min at 37 °C. In a separate microcentrifuge tube, 40S subunits were mixed with a leaderless mRNA encoding the start (methionine) codon (AUG) in the P-site and either a phenylalanine codon (UUC, marked F in Extended Data Fig. 4), a lysine codon (AAA, marked K in Extended Data Fig. 4) or a strong, tetranucleotide stop codon (UAAA, marked X in Extended Data Fig. 4) in the A-site followed by a poly-pyrimidine track of 19 cytidines (for example, for Phe: CCAC-AUG-**UUC**-CCC-CCC-CCC-CCC-CCC-CCC, Integrated DNA Technologies) or by a truncated mRNA with a uridine in the +1 position of the A-site codon (marked +1 in Extended Data Fig. 4; CCAC-AUG-**U**, Integrated DNA Technologies). The 40S and mRNA were incubated for 5 min at 37 °C in 1×10 buffer then with tRNA^{fMet} for 1 min, yielding the following concentrations: 1 µM 40S, 20 µM mRNA and 1.2 µM tRNA^{fMet}. The 40S and 60S solutions were mixed 1:1 and incubated for 5 min at 37 °C to form 80S complexes. The solution was diluted to 200 nM 80S in 1×10 buffer for use as a 10× stock in tRNA cleavage assays. 40S and 60S subunits were also preincubated in 1×10 at 1 µM then diluted to 200 nM in 1×10 buffer for use in subunit-dependence assays.

To assemble different ternary complexes, eEF1A, IVT tRNA^{Ala} or Ala-tRNA^{Ala}, and GTP or GDPCP were assembled in 1×10 buffer with 10 mM βME by preincubation of eEF1A and GTP (Promega) or GDPCP (Jena Bioscience) for 5 min at 37 °C followed by addition of tRNA^{Ala} or Ala-tRNA^{Ala} for 1 min at 37 °C, and were then kept on ice until use. The resulting ternary complex reactions contained 10 µM eEF1A, 2.5 µM tRNA^{Ala} or Ala-tRNA^{Ala}, and 1 mM GTP or GDPCP and were used as a 10× stock in tRNA cleavage assays.

The tRNA cleavage reactions were mixed on ice in 1×10 buffer with 10 mM βME and Triton X-100 and were carried out at 37 °C. The order of addition was 1×10 buffer, Triton X-100 (to 0.01% (v/v) all final concentration), rRNasin (to 0.8 U µl^{-1}), 80S ribosomal complex (to 20 nM), angiogenin (to 10 nM), then, to start the reaction, tRNA^{Ala}, Ala-tRNA^{Ala}, eEF1A–tRNA^{Ala}–GTP, eEF1A–Ala-tRNA^{Ala}–GTP, eEF1A–Ala-tRNA^{Ala}–GDPCP or total rabbit tRNA as noted (tRNA concentration to a final concentration of 250 nM for tRNA^{Ala}, 250 nM for either 17-mer or 33-mer hairpin, or 0.8 A_{260}/1 cm for total rabbit tRNA). After tRNA addition, the tubes were shifted to 37 °C for the indicated times (0, 1, 10 or 100 min), and then a 10 µl aliquot of the reaction was removed and quenched with 12 µl of 8 M urea loading buffer (8 M urea, 2 mM Tris-HCl pH 8, 20 mM EDTA). When all of the reactions were completed, the reactions were heated at 65 °C for 5 min, centrifuged, vortexed and loaded onto a 15% pre-cast Novex Urea-TBE gel (Thermo Fisher Scientific) and run at 180 V for 60 min alongside small RNA marker (Ab Nova). The gels were stained in 1× TBE with 1:20,000 SYBR Gold nucleic acid stain (Thermo Fisher Scientific) for 5–30 min. The stained gels were imaged on the ChemiDoc MP system (Bio-Rad Laboratories) using the SYBR Gold setting. The resulting raw .tiff images were analysed in Fiji[93] using the Band/Peak Quantification Tool Macro[94] to measure the signal from tRNA fragments and to the full-length tRNA. Data were exported to Microsoft Excel 16, in which the ratio of signal from tRNA fragments to full-length tRNA was calculated and then exported for graphing in Prism 8 or Prism 9 (GraphPad Software).

Northern blotting

After SYBR Gold staining and detection, the nucleic acids on 15% urea–PAGE gels were transferred to the BrightStar-Plus Positively Charged Nylon Membrane (Thermo Fisher Scientific) through semi-dry transfer in 0.5× TBE at 200 mA for 30 min. The membranes were UV cross-linked (Stratalinker; automatic setting) and, after drying, were prehybridized with ULTRAhyb-Oligo solution (Thermo Fisher Scientific) for 1 h at 40 °C. The membranes were then hybridized with 100 nM 5′ biotinylated DNA probes (anti-yeast 5′ tRNA^{Ala}: 5′ATGCTAAGGGAGCGCGCTACC GACTACGCCACACGCCC; anti-rabbit 5′ tRNA$^{Asp}_{GTC}$: GTGACAGGCGGGG ATACTCACCACTATACTAACGAGGA; anti-rabbit 5′tRNA$^{Gly}_{GCC}$ GTGGCAGG CGAGAATTCTACCACTGAACCACCAATGC; anti-rabbit 5′ tRNA^{his}:

GCCACAACGCAGAGTACTAACCACTATACGATCACGGC, Integrated DNA Technologies) in ULTRAhyb-oligo solution for 1 h (yeast $tRNA^{ala}$) or overnight (rabbit tRNAs) at 37 °C. The rabbit tRNA probes were designed by consulting the GtRNAdb entries for *O. cuniculus*[95] and finding the most common and similar tRNA gene sequences matching previously characterized human tRNA targets of angiogenin[12,31]. The membranes were washed twice at room temperature with 2× SSC + 0.1% SDS, and the probes were then detected using the Chemiluminescent Nucleic Acid Detection Module Kit (Thermo Fisher Scientific). The stained gels were imaged on a ChemiDoc MP system (Bio-Rad Laboratories) using the chemiluminescence setting.

Reporting summary

Further information on research design is available in the Nature Portfolio Reporting Summary linked to this article.

Data availability

The structural models generated in this study have been deposited in the RCSB Protein Data Bank under the following accession codes: 9BDL (rabbit 80S ribosome with angiogenin), 9BDN (rabbit ribosome with angiogenin and $tRNA^{Ala}$) and 9BDP (rabbit ribosome with angiogenin and Ala-$tRNA^{Ala}$ bound to eEF1A). The cryo-EM maps used to generate models in this study have been deposited in the Electron Microscopy Data Bank under the following accession codes: EMD-44461 (rabbit 80S ribosome with angiogenin), EMD-44463 (rabbit 80S ribosome with angiogenin and $tRNA^{Ala}$), EMD-44464 (rabbit 80S ribosome with angiogenin and Ala-$tRNA^{Ala}$ bound to eEF1A). Additional cryo-EM maps have been deposited in the Electron Microscopy Data Bank under the following accession codes: EMD-44457 (80S ribosome with angiogenin in RRL), EMD-44458 (rabbit 80S ribosome with angiogenin, in vitro complex assembled without substrate $tRNA^{Ala}$), EMD-44459 (rabbit 80S ribosome with angiogenin(H13A)), EMD-44460 (rabbit 80S ribosome with angiogenin(H13A) and $tRNA^{Ala}$). The coordinate files used in this study are available at the PDB: 7TOR, 5EOP, 1EHZ, 5LZS, 5UYM, 1A4Y and 5RSA; or from the AlphaFold Protein Structure Database (https://alphafold.ebi.ac.uk/entry/P02994; https://alphafold.ebi.ac.uk/entry/P02994)[85,86]. The electron density map used in this study is available from the Electron Microscopy Database (EMD-4729).

62. Sievers, F. et al. Fast, scalable generation of high-quality protein multiple sequence alignments using Clustal Omega. *Mol. Syst. Biol.* **7**, 539 (2011).
63. Madeira, F. et al. Search and sequence analysis tools services from EMBL-EBI in 2022. *Nucleic Acids Res.* **50**, W276–W279 (2022).
64. Kurachi, K., Davie, E. W., Strydom, D. J., Riordan, J. F. & Vallee, B. L. Sequence of the cDNA and gene for angiogenin, a human angiogenesis factor. *Biochemistry* **24**, 5494–5499 (1985).
65. Yoon, J. M., Kim, S. H., Kwon, O. B., Han, S. H. & Kim, B. K. High level expression of soluble angiogenin in *Escherichia coli*. *IUBMB Life* **47**, 267–273 (1999).
66. Holloway, D. E., Hares, M. C., Shapiro, R., Subramanian, V. & Acharya, K. R. High-level expression of three members of the murine angiogenin family in *Escherichia coli* and purification of the recombinant proteins. *Protein Expr. Purif.* **22**, 307–317 (2001).
67. Shapiro, R. et al. Expression of Met-(−1) angiogenin in *Escherichia coli*: conversion to the authentic. *Anal. Biochem.* **175**, 450–461 (1988).
68. Abeyrathne, P. D., Koh, C. S., Grant, T., Grigorieff, N. & Korostelev, A. A. Ensemble cryo-EM uncovers inchworm-like translocation of a viral IRES through the ribosome. *eLife* **5**, e14874 (2016).
69. Walker, S. E. & Fredrick, K. Preparation and evaluation of acylated tRNAs. *Methods* **44**, 81–86 (2008).
70. Eyler, D. E. & Green, R. Distinct response of yeast ribosomes to a miscoding event during translation. *RNA* **17**, 925–932 (2011).
71. Skogerson, L. & Engelhardt, D. Dissimilarity in protein chain elongation factor requirements between yeast and rat liver ribosomes. *J. Biol. Chem.* **252**, 1471–1475 (1977).
72. Loveland, A. B. et al. Ribosome inhibition by C9ORF72-ALS/FTD-associated poly-PR and poly-GR proteins revealed by cryo-EM. *Nat. Commun.* **13**, 2776 (2022).
73. England, C. G., Ehlerding, E. B. & Cai, W. NanoLuc: a small luciferase is brightening up the field of bioluminescence. *Bioconjug. Chem.* **27**, 1175–1187 (2016).
74. Susorov, D., Egri, S. & Korostelev, A. A. Termi-Luc: a versatile assay to monitor full-protein release from ribosomes. *RNA* https://doi.org/10.1261/rna.076588.120 (2020).
75. Mastronarde, D. N. Automated electron microscope tomography using robust prediction of specimen movements. *J. Struct. Biol.* **152**, 36–51 (2005).
76. Svidritskiy, E., Demo, G., Loveland, A. B., Xu, C. & Korostelev, A. A. Extensive ribosome and RF2 rearrangements during translation termination. *eLife* **8**, e46850 (2019).
77. Kremer, J. R., Mastronarde, D. N. & McIntosh, J. R. Computer visualization of three-dimensional image data using IMOD. *J. Struct. Biol.* **116**, 71–76 (1996).
78. Grant, T., Rohou, A. & Grigorieff, N. cisTEM, user-friendly software for single-particle image processing. *eLife* **7**, e35383 (2018).
79. Lyumkis, D., Brilot, A. F., Theobald, D. L. & Grigorieff, N. Likelihood-based classification of cryo-EM images using FREALIGN. *J. Struct. Biol.* **183**, 377–388 (2013).
80. Shanmuganathan, V. et al. Structural and mutational analysis of the ribosome-arresting human XBP1u. *eLife* **8**, e46267 (2019).
81. Tang, G. et al. EMAN2: an extensible image processing suite for electron microscopy. *J. Struct. Biol.* **157**, 38–46 (2007).
82. Pettersen, E. F. et al. UCSF Chimera—a visualization system for exploratory research and analysis. *J. Comput. Chem.* **25**, 1605–1612 (2004).
83. Emsley, P. & Cowtan, K. Coot: model-building tools for molecular graphics. *Acta Crystallogr. D* **60**, 2126–2132 (2004).
84. Shi, H. & Moore, P. B. The crystal structure of yeast phenylalanine tRNA at 1.93 Å resolution: a classic structure revisited. *RNA* **6**, 1091–1105 (2000).
85. Varadi, M. et al. AlphaFold Protein Structure Database: massively expanding the structural coverage of protein-sequence space with high-accuracy models. *Nucleic Acids Res.* **50**, D439–D444 (2022).
86. Jumper, J. et al. Highly accurate protein structure prediction with AlphaFold. *Nature* **596**, 583–589 (2021).
87. Korostelev, A., Bertram, R. & Chapman, M. S. Simulated-annealing real-space refinement as a tool in model building. *Acta Crystallogr. D* **58**, 761–767 (2002).
88. Chapman, M. S. Restrained real-space macromolecular atomic refinement using a new resolution-dependent electron-density function. *Acta Crystallogr. A* **51**, 69–80 (1995).
89. Zhou, G., Wang, J., Blanc, E. & Chapman, M. S. Determination of the relative precision of atoms in a macromolecular structure. *Acta Crystallogr. D* **54**, 391–399 (1998).
90. Adams, P. D. et al. The Phenix software for automated determination of macromolecular structures. *Methods* **55**, 94–106 (2011).
91. Afonine, P. V. et al. Real-space refinement in PHENIX for cryo-EM and crystallography. *Acta Crystallogr. D* **74**, 531–544 (2018).
92. DeLano, W. L. The PyMOL molecular graphics system (DeLano Scientific, 2002).
93. Schindelin, J. et al. Fiji: an open-source platform for biological-image analysis. *Nat. Methods* **9**, 676–682 (2012).
94. Ohgane, K. & Yoshioka, H. Quantification of gel bands by an Image J macro, band/peak quantification tool. *protocols.io*, https://doi.org/10.17504/protocols.io.7vghn3w (2019).
95. Chan, P. P. & Lowe, T. M. GtRNAdb: a database of transfer RNA genes detected in genomic sequence. *Nucleic Acids Res.* **37**, D93–D97 (2009).
96. Williams, C. J. et al. MolProbity: more and better reference data for improved all-atom structure validation. *Protein Sci.* **27**, 293–315 (2018).

Acknowledgements We thank C. Xu, J.-Y. Chang and C. Ouch for data collection at the cryo-EM facility at UMass Medical School; E. Sholi for help with protein purification; D. Conte Jr for comments on the manuscript; and the members of the Jacobson and Korostelev laboratories for discussions. This study was supported by grants from the US National Institutes of Health 1R35GM122468 to A.J. and R35 GM127094 to A.A.K.

Author contributions Conceptualization: A.B.L. and A.A.K. Methodology: A.B.L., A.J. and A.A.K. Validation: A.B.L. and A.A.K. Investigation: A.B.L. and R.G. Resources: A.B.L., R.G., C.S.K., A.J. and A.A.K. Writing—original draft: A.B.L and A.A.K. Writing—review and editing: A.B.L., C.S.K., A.J. and A.A.K. Visualization: A.B.L. Supervision. A.A.K. Funding acquisition: A.A.K.

Competing interests A.J. is co-founder, director and consultant for PTC Therapeutics. The other authors declare no competing interests.

Additional information

Supplementary information The online version contains supplementary material available at https://doi.org/10.1038/s41586-024-07508-8.

Correspondence and requests for materials should be addressed to Anna B. Loveland or Andrei A. Korostelev.

Peer review information *Nature* thanks the anonymous reviewers for their contribution to the peer review of this work.

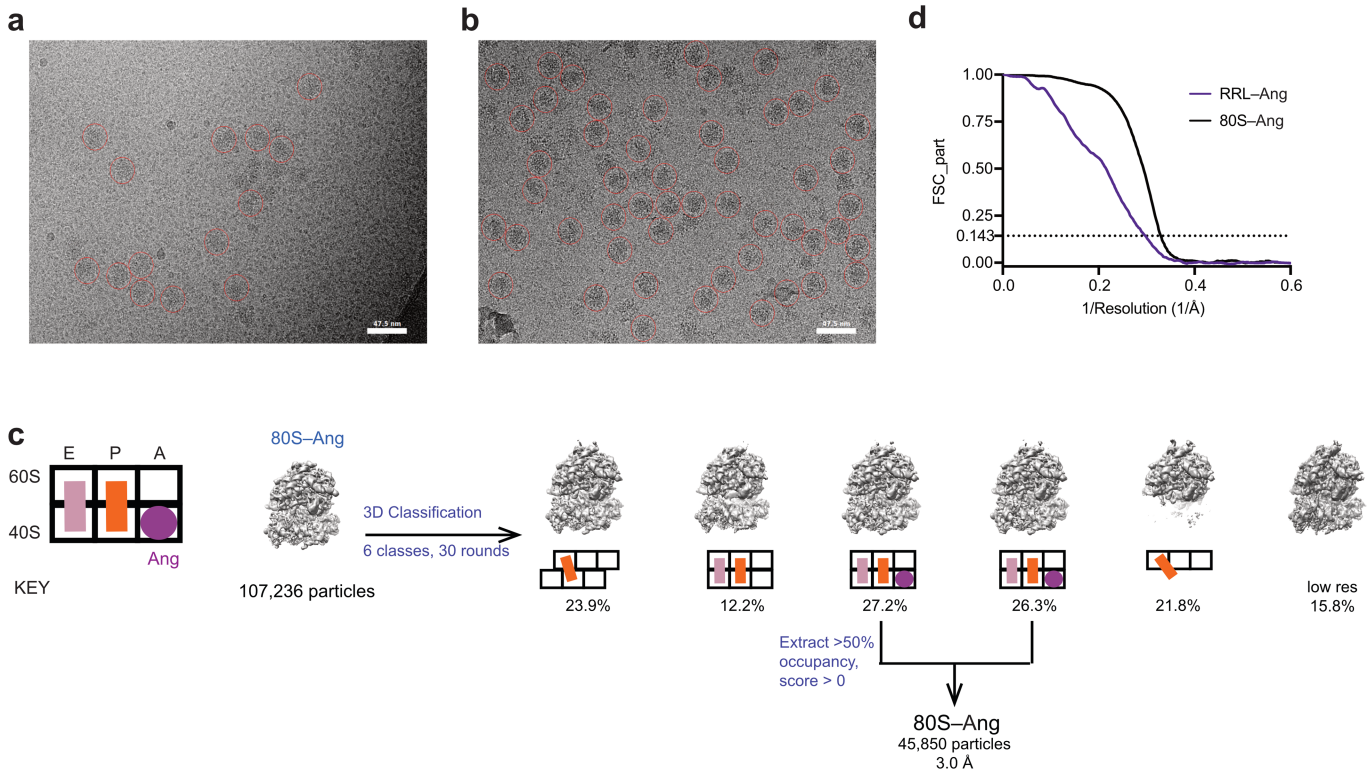

Extended Data Fig. 1 | See next page for caption.

Extended Data Fig. 1 | Cryo-EM characterization of angiogenin interactions with the ribosome. (**a**) Example of hand-picked ribosome particles (red circles) on one of the higher contrast micrographs (n = 600) containing rabbit reticulocyte lysates treated with angiogenin. Representative micrograph had a defocus of −1.4 µm. Notice low contrast of ribosomes among concentrated lysates. (**b**) Examples of automatic particle picking of ribosome in cisTEM (red circles) on a micrograph containing in vitro assembled 80S–angiogenin(H13A) ribosome complexes. Micrograph was taken on same microscope and has similar defocus and CTF fitting resolution criteria to micrograph in (**a**). (**c**) Maximum-likelihood classification in Frealign of a dataset of in vitro assembled 80S ribosome complexes with angiogenin reveals angiogenin bound to the A site of ribosomes in the non-rotated (classical) state. (**d**) Masked, Fourier shell correlation curve as a function of inverse resolution for the map derived from 45,850 particles shown in Extended Data Fig. 1c (FSC_part from Frealign v9) (80S–angiogenin, black) or for the map from rabbit reticulocyte lysates derived from 1,960 particles shown in Fig. 1d,e (RRL–angiogenin, purple). (**e**-**j**) Examples of interactions of angiogenin with the A-site. Model of 80S–angiogenin is shown with the 2.8 Å cryo-EM map, sharpened by a B-factor of −50 Å^2 and shown as mesh at σ levels as noted in individual legends. (**e**) Interaction of angiogenin with H69 of 28S rRNA. Mesh is shown at 2.75 σ. (**f**) Interaction of angiogenin with 18S rRNA. Mesh is shown at 2.75 σ. (**g**) Binding of angiogenin near the universally conserved decoding centre residues of H69 (28S rRNA) and h44 (18S rRNA). Mesh for mRNA is shown at 3 σ; for angiogenin and h44, at 4 σ; and for H69 and G626 at 5 σ. mRNA is green for well modelled residues, grey for disordered residues. (**h**) Interaction of angiogenin with the A-site codon (mRNA is green for well modelled residues, grey for disordered residues). Mesh is shown at 3.5 σ both mRNA and angiogenin. (**i**) Interaction of angiogenin with P-site tRNA. Mesh is shown at 3.75 σ. (**j**) Interactions of angiogenin with the first nucleotide of the A-site codon adjacent to the P-tRNA anticodon and codon interaction. Mesh is shown at 4 σ.

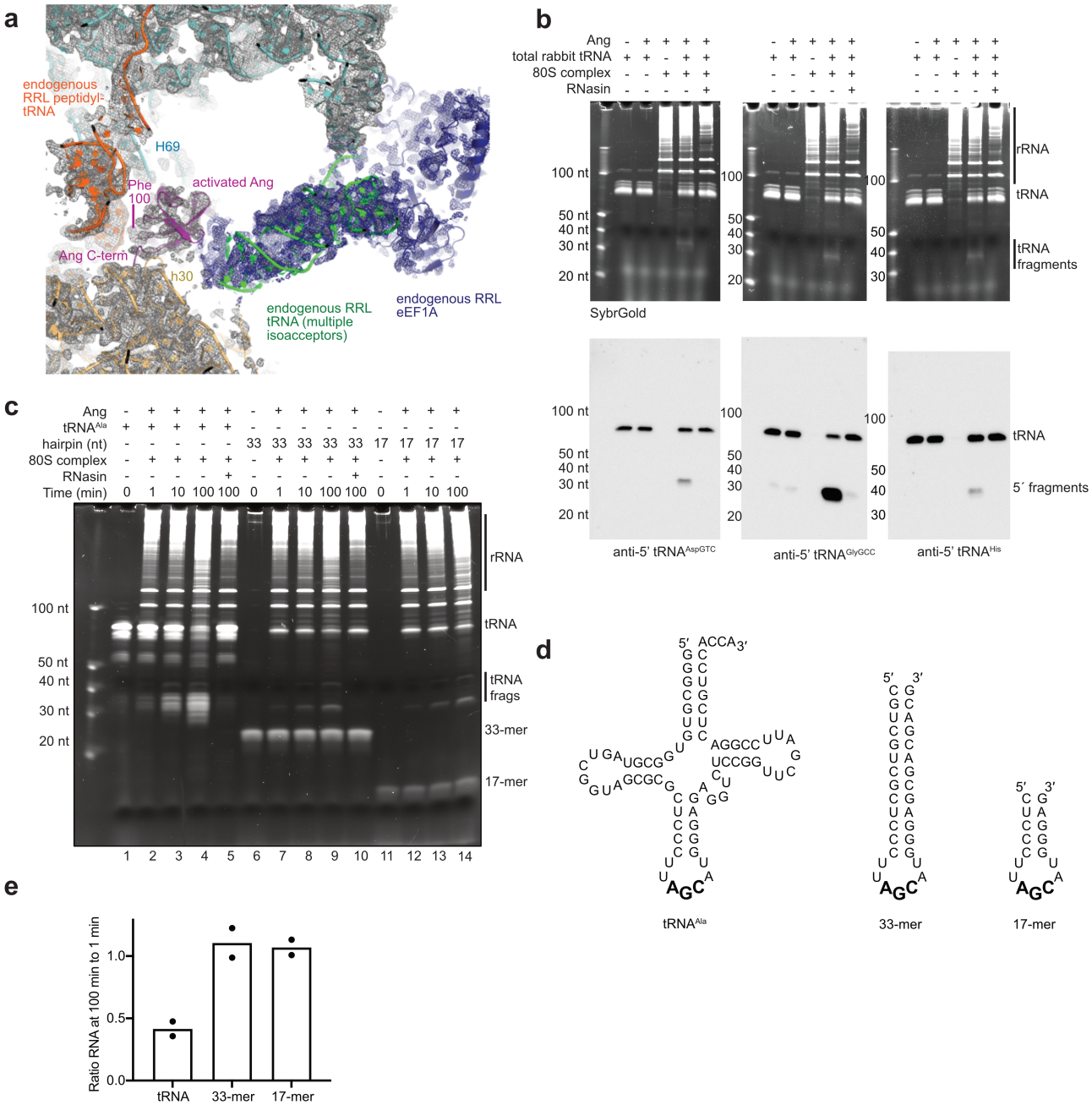

Extended Data Fig. 2 | Angiogenin cleaves various tRNAs but not isolated stem loops. (**a**) Rigid-body docking of in vitro assembled 80S–angiogenin–Ala-tRNA^{Ala}–eEF1A–GDPCP model into the RRL–angiogenin cryo-EM map (grey mesh at 6 σ for most of complex, but due to sub-stoichiometry, blue mesh at 4 σ for ternary complex) shows good agreement of in vitro model with the complex visualized directly in rabbit reticulocyte lysates. The density shows that the C-terminal residues of angiogenin form an extended beta strand in lysates and that the ribosome and ternary complex position the anticodon of tRNA near the active site of angiogenin in lysates. (**b**) Activity of 10 nM angiogenin alone or together with the 80S ribosome complex (including model mRNA encoding phenylalanine) was checked against total rabbit tRNA purified from rabbit reticulocyte lysates. After 100 min, cleavage reactions were separated by denaturing 15% Urea-PAGE gels stained with SYBR Gold (top) then later detected via Northern blotting (bottom) for the 5′ end of three different rabbit tRNA as noted (see Methods). tRNA fragments of all three tRNAs tested increase in the presence of the 80S–angiogenin complex and are prevented by RNasin (n = 2 independent experiments). (**c**) Activity of angiogenin alone or together with the 80S ribosome complex (including tRNA^{fMet} and model mRNA encoding phenylalanine in A site) was checked using in vitro translated yeast tRNA^{Ala}, an extended 33-mer hairpin including the yeast tRNA^{Ala} anticodon stem loop, or a 17-mer including only the yeast tRNA^{Ala} anticodon stem loop (see Extended Data Fig. 2d). At the specified time (in minutes), cleavage reactions were separated by denaturing 15% Urea-PAGE gels stained with SYBR Gold. Full-length tRNA^{Ala} is depleted over time while fragments arise in the presence of the 80S–angiogenin complex, but the 33-mer and 17-mer are not depleted suggesting tRNA is cleaved more effectively than a simple hairpin. Weak tRNA-fragment-sized bands appearing in 33-mer and 17-mer lanes likely arise from tRNA^{fMet,} which is present in the 80S complex for positioning in the P-site. (n = 2 independent experiments). (**d**) Diagrams depicting the secondary structure of in vitro translated yeast tRNA^{Ala}, the extended 33-mer hairpin including the yeast tRNA^{Ala} anticodon stem loop, or the 17-mer hairpin used in Extended Data Fig. 2c. Larger, bold residues are the anticodon of tRNA^{Ala}. (**e**) Quantification of full length tRNA and hairpins from Extended Data Fig. 2c. The amount of full-length tRNA decreased by 50–66% from 1 to 100 min while the amount of hairpins stays constant. (bar shows mean of n = 2 independent experiments).

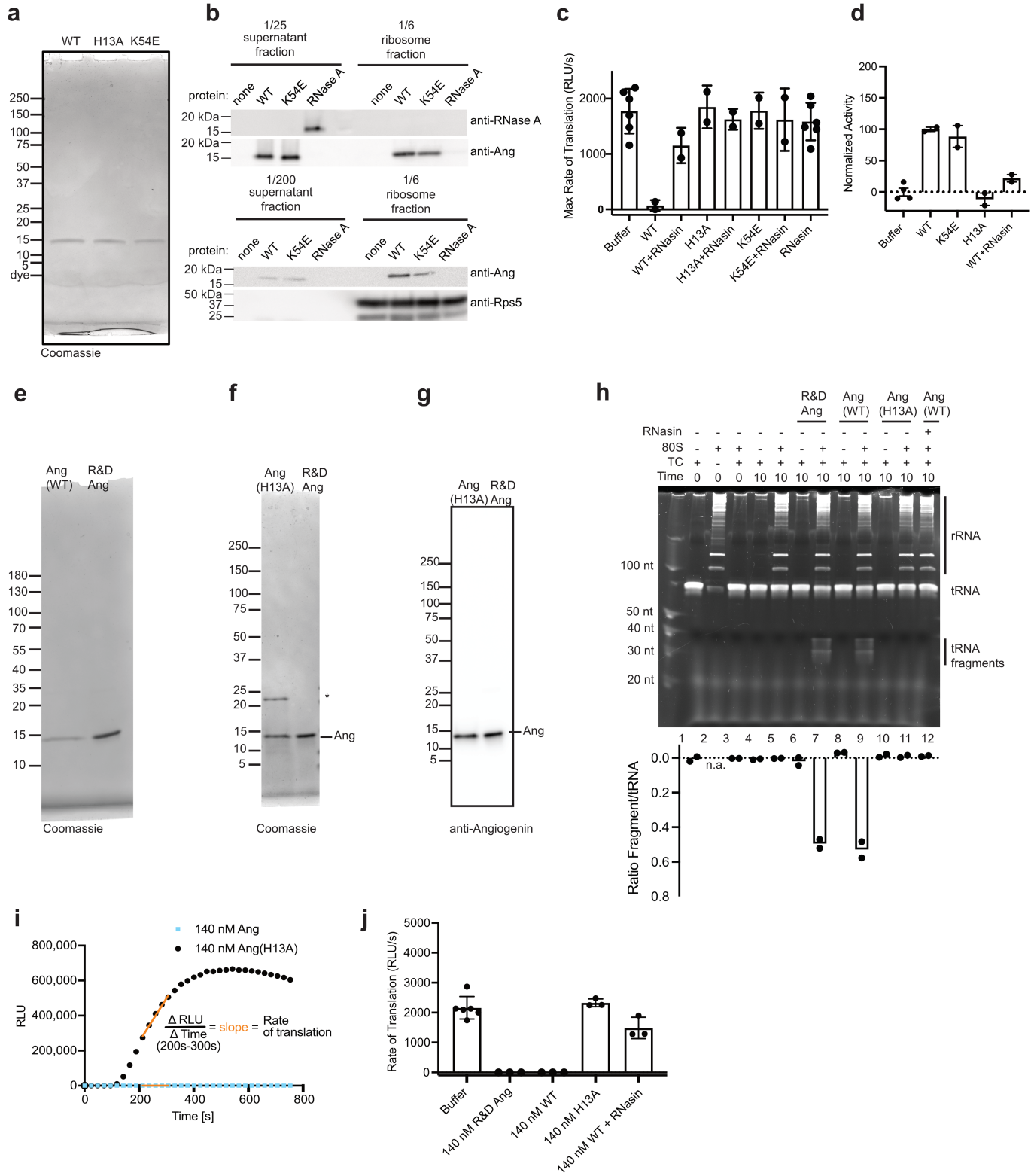

Extended Data Fig. 3 | See next page for caption.

Extended Data Fig. 3 | Purification and characterization of WT, H13A and K54E angiogenin. (**a**) SDS PAGE showing inclusion-body expressed, refolded and purified WT, H13A and K54E angiogenin ("refolded" Angiogenin see Methods, **Preparation of Angiogenin**) (n = 1). (**b**) 200 nM WT refolded angiogenin co-pellets with purified ribosomes more efficiently than angiogenin(K54E). Bovine pancreatic RNase A does not co-pellet with ribosome under these conditions (n = 1). (**c**) RRL translation of nanoluciferase-encoding mRNA is inhibited by 90 nM refolded WT but not H13A or K54E angiogenin. These data, excluding RNasin controls, also appear in Fig. 2k. (mean +/− s.d., n = 2 for mutants or 6 for controls, independent experiments). (**d**) Refolded WT angiogenin and angiogenin(K54E) but not angiogenin(H13A) exhibit weak RNase activity against total yeast tRNA in the absence of ribosomes, at high enzyme concentration and high tRNA concentration[3,44] (50 and 300 times higher, respectively, than in the ribosome-activated cleavage assay), indicating that K54E mutation does not affect the basal catalytic activity (**Methods**) (mean +/− s.e., n = 2 independent experiments). (**e**-**f**) SDS PAGE showing recombinant, soluble WT angiogenin (**e**) and angiogenin(H13A) (**f**) ("soluble" angiogenin, **Methods, Preparation of Angiogenin**) in comparison with 200 ng of R&D angiogenin. * is a contaminant in soluble angiogenin(H13A) prep (n = 1). (**g**) Western blotting of soluble angiogenin(H13A) and R&D angiogenin shows similar amounts are loaded (n = 1). (**h**) Comparison of $tRNA^{Ala}$ cleavage by R&D vs. soluble WT and H13A angiogenin (10 nM). A ternary complex containing Ala-$tRNA^{Ala}$, eEF1A and GDPCP was treated with angiogenin in the presence or absence of the 80S ribosome complex with UUC-containing mRNA and $tRNA^{fMet}$. After 0 or 10 min, cleavage reactions were separated by denaturing 15% Urea-PAGE gels and stained with SYBR Gold. R&D and soluble WT angiogenin exhibit the same activity, while angiogenin(H13A) is inactive. (mean, n = 2 independent experiments). (**i**) Translation of nanoluciferase-encoding mRNA is inhibited by soluble WT angiogenin (similarly to R&D angiogenin shown in Fig. 1a), but not by the soluble angiogenin(H13A) (RLU: relative light units). Example trace is shown. (**j**) Apparent rate of translation, measured as RLU/s (see Extended Data Fig. 3i), in the presence of soluble WT angiogenin or angiogenin(H13A), (mean +/− s.d., n = 3 independent experiments except buffer control which was duplicated for n = 6).

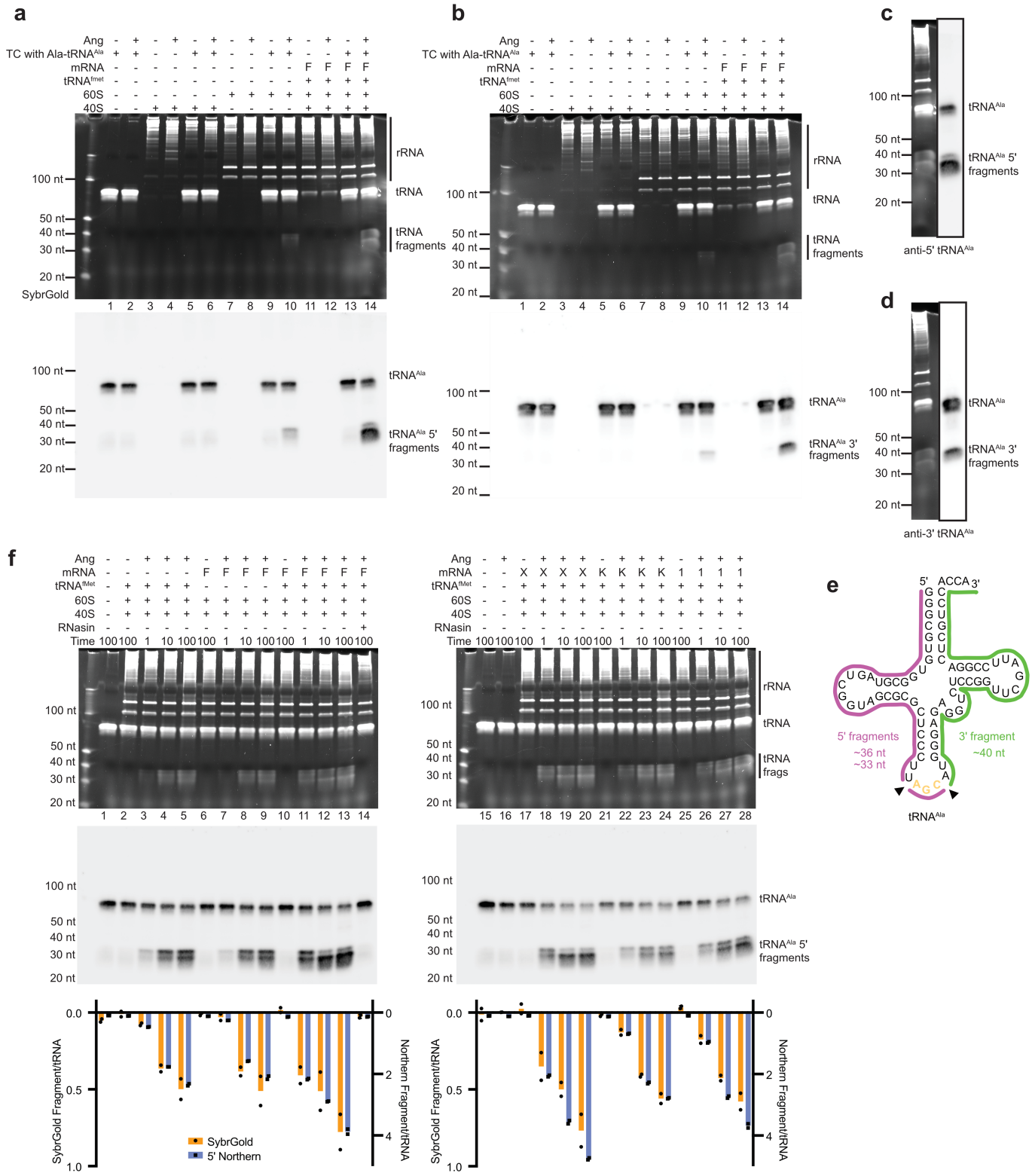

Extended Data Fig. 4 | See next page for caption.

Extended Data Fig. 4 | Effects of ribosome complex composition on angiogenin activation. (**a**) Production of $tRNA^{Ala}$ fragments by angiogenin is stimulated by an elongation-like 80S ribosome complex more efficiently than by 40S or 60S subunits. A ternary complex containing Ala-$tRNA^{Ala}$, eEF1A and GDPCP was supplemented to 80S ribosome complexes assembled using 40S, 60S, leaderless mRNA placing phenylalanine UUC codon in A site, $tRNA^{fMet}$ complementary to the P-site, and/or angiogenin. After 10 min, cleavage reactions were separated by denaturing 15% Urea-PAGE gels stained with SYBR Gold (top) then later detected via Northern blotting for the 5′ end of yeast $tRNA^{Ala}$ (bottom), n = 2 independent experiments. (**b**) Same reactions as in (**a**) run separately then probed for the 3′ end of yeast $tRNA^{Ala}$, n = 2 independent experiments. (**c**) Close-up of lane 14 from (**a**) showing SYBR Gold and 5′ Northern side-by-side. Two 5′ tRNA fragments are apparent with the more intense one running above the 30 nt marker. (**d**) Close-up of lane 14 from (**b**) showing SYBR Gold and 3′ Northern side-by-side. 3′ tRNA fragment runs close to the 40 nt marker. (**e**) Secondary structure diagram of $tRNA^{Ala}$ with the anticodon shown in orange font. Triangles indicate potential cleavage locations in the anticodon stem based on preference of angiogenin to cleaved at pyrimidine-adenine dinucleotides[52]. (**f**) Cleavage of $tRNA^{Ala}$ by angiogenin is stimulated by multiple 80S ribosome complexes including ones lacking mRNA, lacking P-site tRNA, and ones encoding amino acids phenylalanine (F, UUC) or lysine (K, AAA), or a stop codon (X, UAA) as well as by truncated mRNA (1, single uridine in A site). A ternary complex Ala-$tRNA^{Ala}$, eEF1A and GDPCP was supplemented to ribosome complexes assembled using 40S, 60S, mRNAs as specified, $tRNA^{fMet}$ complementary to the P-site, and/or angiogenin, and after the indicated time (in minutes) cleavage reactions were stopped then separated by denaturing 15% Urea-PAGE gels stained with SYBR Gold (top) then later detected via Northern blotting (bottom) for the 5′ end of yeast $tRNA^{Ala}$. (mean, n = 2 independent experiments).

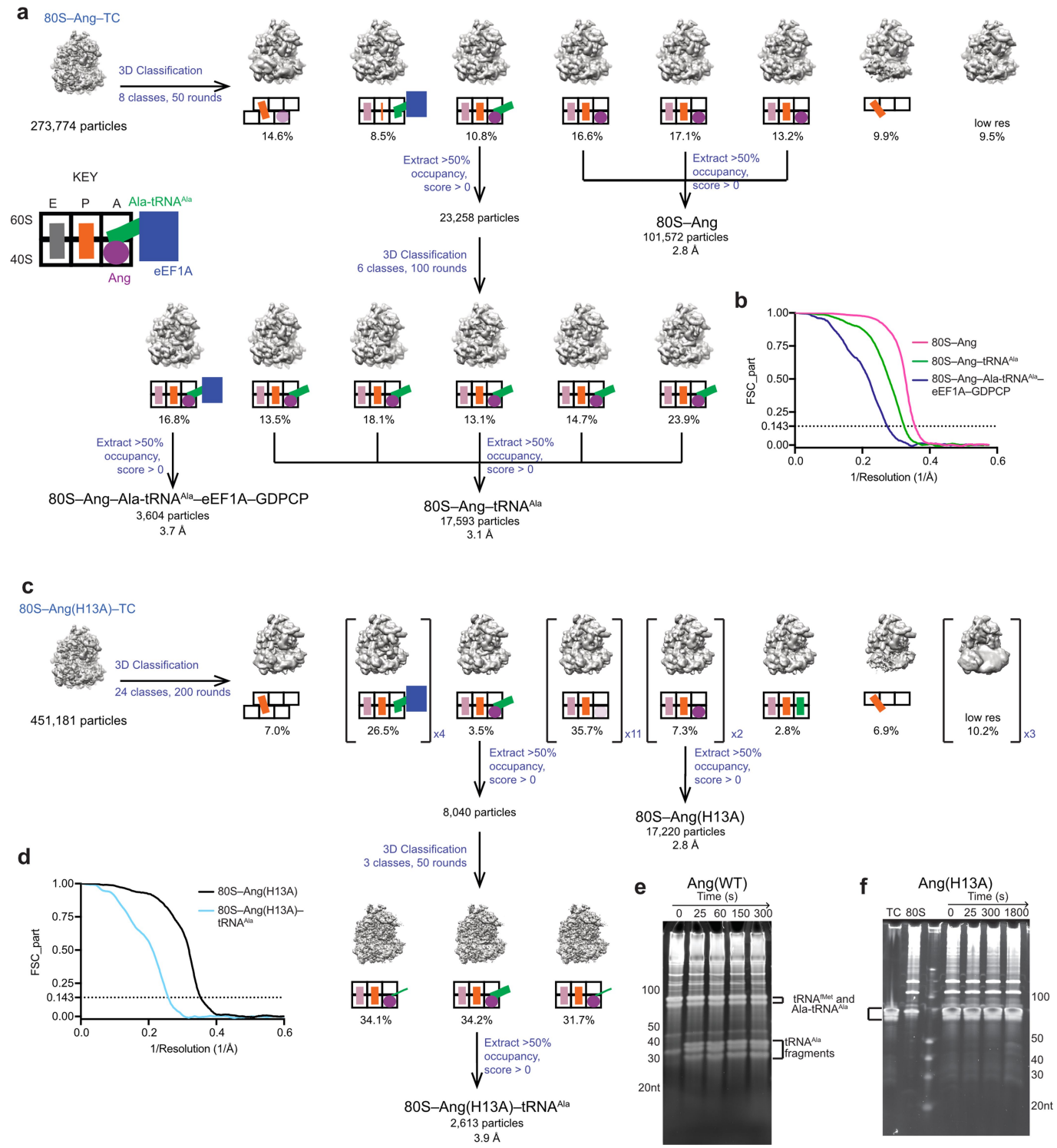

Extended Data Fig. 5 | See next page for caption.

Extended Data Fig. 5 | Cryo-EM of the 80S–angiogenin and 80S–angiogenin(H13A) complexes with Ala-tRNA^{Ala}–eEF1A–GDPCP ternary complex. (**a**) Maximum-likelihood classification in Frealign of a dataset of 80S ribosome with angiogenin and ternary complex of Ala-tRNA^{Ala}–eEF1A–GDPCP reveals classes with angiogenin bound to the ribosomal A site as tRNA is presented to the angiogenin active site. (**b**) Masked, Fourier shell correlation curves (FSC) as a function of inverse resolution for the cryo-EM map described in Extended Data Fig. 5a. (**c**) Maximum-likelihood classification in Frealign of a dataset collected from 80S ribosomes with recombinantly expressed angiogenin(H13A) and ternary complex of Ala-tRNA^{Ala}–eEF1A–GDPCP. (**d**) Masked, Fourier shell correlation curves (FSC) as a function of inverse resolution for the cryo-EM maps described in Extended Data Fig. 5c. (**e**) Half reactions for assembling the cryo-EM complexes in Extended Data Fig. 5a (Half reaction 1: 80S ribosome complexes with angiogenin; Half reaction 2: ternary complex of Ala-tRNA^{Ala}–eEF1A–GDPCP as described in Methods) were mixed in test tubes held on wet ice. After the indicated time, the reactions were quenched with 8 M Urea loading buffer. For the 0-s time point, Half reaction 1 and Half reaction 2 were added directly to 8 M Urea loading buffer. The reactions were separated on a 15% Urea-PAGE gel to visualize full length and newly cleaved tRNA. tRNA is cleaved nearly maximally by 25 s on ice under these conditions, which mimic the conditions used to prepare cryo-EM grids (n = 1). (**f**) Half reactions for assembling the cryo-EM complexes in Extended Data Fig. 5c (Half reaction 1: 80S ribosome complexes with recombinant angiogenin(H13A); Half reaction 2: ternary complex of Ala-tRNA^{Ala}–eEF1A–GDPCP as described in Methods) were mixed in test tubes at 30 °C. After the indicated time, the reactions were quenched with 8 M Urea loading buffer and separated showing lack of tRNA cleavage under these conditions, which mimic the conditions used to prepare cryo-EM grids (300 s) (n = 1).

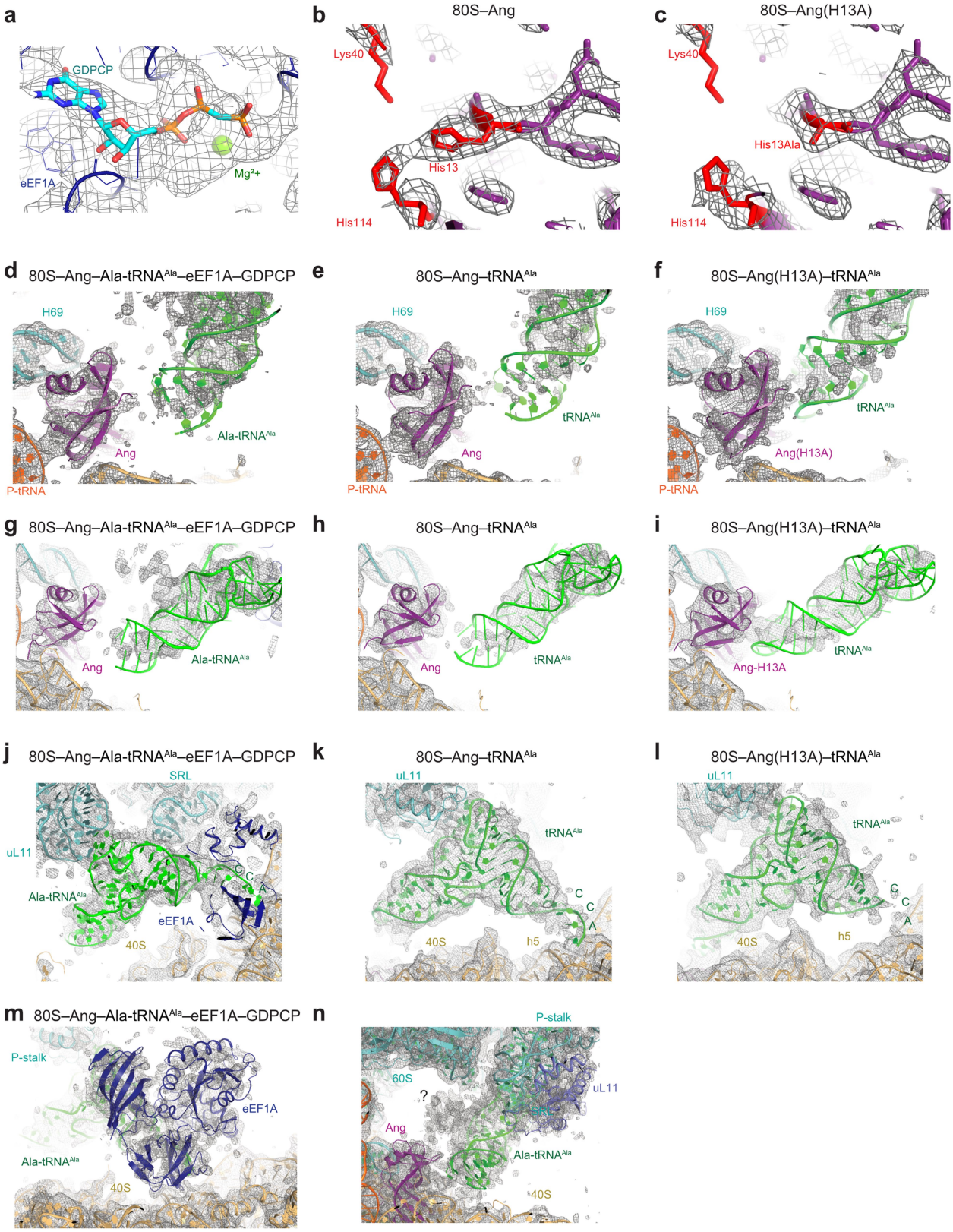

Extended Data Fig. 6 | See next page for caption.

Extended Data Fig. 6 | Cryo-EM density maps of the 80S–angiogenin(WT) and angiogenin(H13A) complexes formed with Ala-tRNA^{Ala}–eEF1A–GDPCP. (**a**) 3.7-Å cryo-EM map of 80S–angiogenin(WT)–Ala-tRNA^{Ala}–eEF1A–GDPCP has density consistent with GDPCP (cyan) bound to eEF1A (blue). GDPCP-bound bacterial EF-Tu (cyan) (PDB: 5UYM) was aligned via the homologous domain 1 to domain 1 of eEF1A. Mesh is shown at 2.75 σ. (**b**). The 2.8-Å cryo-EM map of 80S–angiogenin (WT), sharpened by a B-factor of −50 Å^2, has well-resolved density for the active site residue H13. Mesh is shown at 4 σ. (**c**) The 2.8-Å cryo-EM map of 80S–angiogenin(H13A) (no sharpening) has well-resolved density for the active site of angiogenin supporting mutation of histidine 13 to alanine (H13A) (mesh). The H13A map was rigid-body fitted with our 80S–angiogenin model. Mesh is shown at 4 σ. (**d**-**f**) Comparison of density for tRNA^{Ala} in the 3.7-Å cryo-EM map of 80S–angiogenin(WT)–Ala-tRNA^{Ala}–eEF1A–GDPCP (**d**), 3.1-Å cryo-EM map of 80S–angiogenin(WT)–tRNA^{Ala} (**e**) or 3.9-Å cryo-EM map of 80S–angiogenin(H13A)–tRNA^{Ala} (**f**) show that the anticodon stem–loop (ASL) of tRNA is strongest in the H13A map with the catalytically inactive angiogenin. The cryo-EM maps (grey mesh) are shown without sharpening at 4 σ. (**g**-**i**) Comparison of cryo-EM density filtered to 5 Å in the cryo-EM maps of 80S–angiogenin(WT)–Ala-tRNA^{Ala}–eEF1A–GDPCP (**g**), 80S–angiogenin(WT)–tRNA^{Ala} (**h**) or 80S–angiogenin(H13A)–tRNA^{Ala} (**i**) further supports that the ASL of tRNA is stronger in the H13A map with catalytically inactive angiogenin. (**j**-**l**) The cryo-EM maps of 80S–angiogenin(WT)–Ala-tRNA^{Ala}–eEF1A–GDPCP (**j**), 80S–angiogenin(WT)–tRNA^{Ala} (**k**) or 80S–angiogenin(H13A)–tRNA^{Ala} (**l**) show an L-shaped density consistent with tRNA interacting with the P-stalk via the tRNA elbow. The cryo-EM maps were each low-pass filtered to 5 Å and shown at 3 σ. (**m**) Cryo-EM map of 80S–angiogenin–Ala-tRNA^{Ala}–eEF1A–GDPCP shows density for eEF1A (blue) bound to the shoulder of the 40S (gold). The cryo-EM map was low-pass filtered to 5 Å and is shown at 2.7 σ. (**n**) The cryo-EM map of 80S–angiogenin–Ala-tRNA^{Ala}–eEF1A–GDPCP has an unidentified low-resolution density (question mark) next to the anticodon arm of Ala-tRNA^{Ala} (green) and the P-stalk (uL11, light blue is labelled for reference), which may correspond to a dynamic element of the P-stalk. The cryo-EM map was low-pass filtered to 5 Å and is shown at 2.5 σ.

Extended Data Table 1 | Cryo-EM data collection, refinement and validation statistics

	RRL–Ang	80S–Ang alone	80S–Ang	80S–Ang –tRNA^{Ala}	80S–Ang –Ala-tRNA^{Ala}–eEF1A	80S–Ang (H13A)	80S–Ang (H13A)–tRNA^{Ala}
EMDB Accession ID	44457	44458	44461	44463	44464	44459	44460
PDB Accession ID			9BDL	9BDN	9BDP		
Data collection and processing							
Magnification	60,241x	57,471x	57,471x	57,471x	57,471x	60,241x	60,241x
Voltage (kV)	300	200	200	200	200	300	300
Electron exposure (e^{-}/Å^2)	30	30	30	30	30	30	30
Defocus range (μm)	0.3-2.1	0.4-3	0.3-3.7	0.3-3.7	0.3-3.7	0.3-3.7	0.3-3.7
Pixel size (Å)	0.83	0.87	0.87	0.87	0.87	0.83	0.83
Symmetry imposed	C1	C1	C1	C1	C1	C1	C1
Initial particle images (no.)	6,216	107,236	273,774	273,774	273,774	451,181	451,181
Final particle images (no.)	1,960	45,850	101,572	17,593	3,604	17,220	2,613
Map resolution (Å)**	3.36	3.04	2.81	3.09	3.67	2.84	3.88
FSC threshold	0.143	0.143	0.143	0.143	0.143	0.143	0.143
Map resolution range (Å)	3.0 - >8	2.7 - >8	2.2 - >8	2.8 - >8	3.1 - >8	2.3 - > 8	3.3 - >8
Refinement							
Initial model used (PDB code)	Not modeled	Not modeled	7TOR	7TOR	7TOR	Not modeled	Not modeled
Model resolution (Å)*			2.8	3.1	3.7		
FSC threshold			0.143	0.143	0.143		
Model resolution range (Å)			2.4 - >8	2.8 - >8	3.2 - >8		
Correlation Coefficient (cc_mask)*			0.90	0.87	0.81		
Real-space R-factor †			0.17	0.18	0.20		
Map-sharpening *B* factor (Å^2)			0	0	0		
Model composition*							
Non-hydrogen atoms			212,932	217,113	220,398		
Protein residues			11,336	11,685	12,115		
RNA residues			5,683	5,754	5,753		
B factors (Å^2)*							
Protein			110.5	125.9	152.4		
RNA			113.6	128.8	148.2		
R.m.s. deviations*,§							
Bond lengths (Å)			0.007	0.005	0.005		
Bond angles (°)			0.76	0.75	0.87		
Validation*							
MolProbity score			1.76	1.79	1.96		
Clashscore			8.70	8.14	10.13		
Poor rotamers (%)			0.1	0.09	0.37		
Ramachandran plot*							
Favored (%)			95.82	95.03	93.41		
Allowed (%)			4.14	4.93	6.59		
Disallowed (%)			0.04	0.04	0.0		
Validation (RNA)*							
Good sugar pucker (%)			98.9	99.2	99.1		
Good backbone (%)#			72.7	81.7	76.2		

* Statistics calculated by Phenix vs. 1.14[90,91]. ** FSC_part from Frealign v. 9.11[79]. † from RSRef. § root mean square deviations. # RNA backbone suites that fall into recognized rotamer conformations defined by Molprobity[96].

nature portfolio

Corresponding author(s): Anna B. Loveland
Andrei A Korostelev

Last updated by author(s): 06/10/2024

Reporting Summary

Nature Portfolio wishes to improve the reproducibility of the work that we publish. This form provides structure for consistency and transparency in reporting. For further information on Nature Portfolio policies, see our Editorial Policies and the Editorial Policy Checklist.

Statistics

For all statistical analyses, confirm that the following items are present in the figure legend, table legend, main text, or Methods section.

n/a	Confirmed	
☐	☒	The exact sample size (*n*) for each experimental group/condition, given as a discrete number and unit of measurement
☐	☒	A statement on whether measurements were taken from distinct samples or whether the same sample was measured repeatedly
☒	☐	The statistical test(s) used AND whether they are one- or two-sided *Only common tests should be described solely by name; describe more complex techniques in the Methods section.*
☒	☐	A description of all covariates tested
☐	☒	A description of any assumptions or corrections, such as tests of normality and adjustment for multiple comparisons
☐	☒	A full description of the statistical parameters including central tendency (e.g. means) or other basic estimates (e.g. regression coefficient) AND variation (e.g. standard deviation) or associated estimates of uncertainty (e.g. confidence intervals)
☒	☐	For null hypothesis testing, the test statistic (e.g. *F*, *t*, *r*) with confidence intervals, effect sizes, degrees of freedom and *P* value noted *Give P values as exact values whenever suitable.*
☒	☐	For Bayesian analysis, information on the choice of priors and Markov chain Monte Carlo settings
☒	☐	For hierarchical and complex designs, identification of the appropriate level for tests and full reporting of outcomes
☒	☐	Estimates of effect sizes (e.g. Cohen's *d*, Pearson's *r*), indicating how they were calculated

Our web collection on statistics for biologists contains articles on many of the points above.

Software and code

Policy information about availability of computer code

Data collection	Tecan Infinite m1000 pro luminescence reader with Tecan software, Spark® microplate reader (Tecan Trading AG, Switzerland), NanoDrop One, SerialEM (vs. 3.6), IMOD (vs. 4.9.0), ChemiDoc MP system (Bio-Rad Laboratories Inc)
Data analysis	Graphpad Prism 8 and Prism 9, cisTEM (version 1.0-beta and pre-release), Frealign v. 9.11 (Aug 2017 release), EMAN(vs.2.07), RSRef(2000), Phenix (1.16-3549, 1.14-3260, 1.21.-5207), Chimera (vs. 1.7), MacPyMOL: PyMOL v1.7.0.5 enhanced for MacOsX, IMOD (vs. 4.9.0), Microsoft Excel (2007 and vs. 16.81), ClustalOmega (2022), FIJI (ImageJ 1.53t with BandPeakQuantification v.1 plug-in tool)

For manuscripts utilizing custom algorithms or software that are central to the research but not yet described in published literature, software must be made available to editors and reviewers. We strongly encourage code deposition in a community repository (e.g. GitHub). See the Nature Portfolio guidelines for submitting code & software for further information.

Data

Policy information about availability of data

All manuscripts must include a data availability statement. This statement should provide the following information, where applicable:

- Accession codes, unique identifiers, or web links for publicly available datasets
- A description of any restrictions on data availability
- For clinical datasets or third party data, please ensure that the statement adheres to our policy

The structural models generated in this study have been deposited in the RCSB Protein Data Bank under the following accession codes: 9BDL (https://www.rcsb.org/

structure/9BDL) (rabbit 80S ribosome with angiogenin), 9BDN (https://www.rcsb.org/structure/9BDN) (rabbit ribosome with angiogenin and tRNAAla), and 9BDP (https://www.rcsb.org/structure/9BDP) (rabbit ribosome with angiogenin and Ala-tRNAAla bound to eEF1A). The cryo-EM maps used to generate models in this study have been deposited in the Electron Microscopy Database under the following accession codes: EMD-44461 (https://www.ebi.ac.uk/emdb/EMD-44461) (rabbit 80S ribosome with angiogenin), EMD-44463 (https://www.ebi.ac.uk/emdb/EMD-44463) (rabbit 80S ribosome with angiogenin and tRNAAla), EMD-44464 (https://www.ebi.ac.uk/emdb/EMD-44464) (rabbit 80S ribosome with angiogenin and Ala-tRNAAla bound with eEF1A). Additional cryo-EM maps that have been deposited in the Electron Microscopy Database under the following accession codes: EMD-44457 (https://www.ebi.ac.uk/emdb/EMD-44457) (80S ribosome with angiogenin in rabbit reticulocyte lysates), EMD-44458 (https://www.ebi.ac.uk/emdb/EMD-44458) (rabbit 80S ribosome with angiogenin, in vitro complex assembled without substrate tRNAAla), EMD-44459 (https://www.ebi.ac.uk/emdb/EMD-44459) (rabbit 80S ribosome with H13A angiogenin), EMD-44460 (https://www.ebi.ac.uk/emdb/EMD-44460) (rabbit 80S ribosome with H13A angiogenin and tRNAAla).

Research involving human participants, their data, or biological material

Policy information about studies with human participants or human data. See also policy information about sex, gender (identity/presentation), and sexual orientation and race, ethnicity and racism.

Reporting on sex and gender	*Use the terms sex (biological attribute) and gender (shaped by social and cultural circumstances) carefully in order to avoid confusing both terms. Indicate if findings apply to only one sex or gender; describe whether sex and gender were considered in study design; whether sex and/or gender was determined based on self-reporting or assigned and methods used.* *Provide in the source data disaggregated sex and gender data, where this information has been collected, and if consent has been obtained for sharing of individual-level data; provide overall numbers in this Reporting Summary. Please state if this information has not been collected.* *Report sex- and gender-based analyses where performed, justify reasons for lack of sex- and gender-based analysis.*
Reporting on race, ethnicity, or other socially relevant groupings	*Please specify the socially constructed or socially relevant categorization variable(s) used in your manuscript and explain why they were used. Please note that such variables should not be used as proxies for other socially constructed/relevant variables (for example, race or ethnicity should not be used as a proxy for socioeconomic status).* *Provide clear definitions of the relevant terms used, how they were provided (by the participants/respondents, the researchers, or third parties), and the method(s) used to classify people into the different categories (e.g. self-report, census or administrative data, social media data, etc.)* *Please provide details about how you controlled for confounding variables in your analyses.*
Population characteristics	*Describe the covariate-relevant population characteristics of the human research participants (e.g. age, genotypic information, past and current diagnosis and treatment categories). If you filled out the behavioural & social sciences study design questions and have nothing to add here, write "See above."*
Recruitment	*Describe how participants were recruited. Outline any potential self-selection bias or other biases that may be present and how these are likely to impact results.*
Ethics oversight	*Identify the organization(s) that approved the study protocol.*

Note that full information on the approval of the study protocol must also be provided in the manuscript.

Field-specific reporting

Please select the one below that is the best fit for your research. If you are not sure, read the appropriate sections before making your selection.

☒ Life sciences ☐ Behavioural & social sciences ☐ Ecological, evolutionary & environmental sciences

For a reference copy of the document with all sections, see nature.com/documents/nr-reporting-summary-flat.pdf

Life sciences study design

All studies must disclose on these points even when the disclosure is negative.

Sample size	Cryo-EM Datasets for each complex were collected such that a resolution of ~3 A could be reached. Datasets of >100,000 particles were sufficient to reach map resolutions of ~3 A, at which amino acids and nucleotides could be modeled. Datasets of >6,000 particles can produce maps at 3.5 A resolution or better, sufficient to unambiguously assign secondary structure in well-resolved regions.
Data exclusions	A cryo-EM dataset that yielded noisy reconstructions due to bad ice was excluded and the collection was repeated. In vitro cleavage experiments were optimized with different Mg and tRNA substrate concentrations to achieve optimal tRNA cleavage and clear signal. RNase assays with contamination (as judged by band smears throughout the lane) were excluded- these occurred as face mask mandate was dropped. Subsequently assays were repeated with masking.
Replication	For extract and in vitro cleavage experiments, experiments were repeated at least once and up to 3 times. Replicates were independent (separate days, different extract lots from two different sources (Green Hectares and Promega), and multiple lots (R&D) and purification (soluble vs insoluble with refolding) protocols for Angiogenin, and three different ribosome preparations as described in Methods). Replicates were all successful except for technical failures like poor transfer to membranes or torn gels. Cryo-EM experiments were not replicated/ repeated unless map resolution needed to be improved. Multiple but different cryo-EM experiments (ribosome with angiogenin in extracts, in vitro assembled ribosome complex with angiogenin without tRNA substrate, in vitro assembled complex with angiogenin and tRNA substrate, in vitro assembled ribosome complex with H13A angiogenin) all confirm that angiogenin binds to the ribosome.
Randomization	Randomization was not used for biochemical experiments, instead positive and negative controls were used for each type of experiment.

Randomization	Computational approaches to unbiased particle classification (maximum likelihood classification) include randomizations. Classifications were repeated multiple times typically by varying number of classes or mask position.
Blinding	Blinding was not required because for each sample the structural data were all analyzed using the same methods.

Reporting for specific materials, systems and methods

We require information from authors about some types of materials, experimental systems and methods used in many studies. Here, indicate whether each material, system or method listed is relevant to your study. If you are not sure if a list item applies to your research, read the appropriate section before selecting a response.

Materials & experimental systems

n/a	Involved in the study
☐	☒ Antibodies
☒	☐ Eukaryotic cell lines
☒	☐ Palaeontology and archaeology
☒	☐ Animals and other organisms
☒	☐ Clinical data
☒	☐ Dual use research of concern
☒	☐ Plants

Methods

n/a	Involved in the study
☒	☐ ChIP-seq
☒	☐ Flow cytometry
☒	☐ MRI-based neuroimaging

Antibodies

Antibodies used	Mouse anti-angiogenin monoclonal antibody C-1 (sc-74528, Santa Cruz Biotechnologies, Dallas, TX); mouse anti-ribosomal protein s5 monoclonal antibody (A-8) (sc-390935, Santa Cruz Biotechnologies); goat anti-mouse IgG (H+L)-HRP conjugate (62-6520, Thermo Fisher Scientific Corp.), rabbit anti-bovine ribonuclease A polyclonal antibody-peroxidase conjugated (200-4388, Rockland Immunochemicals, Inc., Philadelphia, PA, USA)
Validation	Antibodies were validated against angiogenin and ribosomes obtained from independent sources and validated with appropriate negative controls (see Fig. 1C, Extended Data Fig. 3b). See also the manufacturer's website: https://www.scbt.com/p/ang-i-antibody-c-1 ; https://www.scbt.com/p/ribosomal-protein-s5-antibody-a-8 ; and https://www.thermofisher.com/antibody/product/Goat-anti-Mouse-IgG-H-L-Secondary-Antibody-Polyclonal/62-6520; https://www.rockland.com/datasheet/?code=200-4388

Plants

Seed stocks	*Report on the source of all seed stocks or other plant material used. If applicable, state the seed stock centre and catalogue number. If plant specimens were collected from the field, describe the collection location, date and sampling procedures.*
Novel plant genotypes	*Describe the methods by which all novel plant genotypes were produced. This includes those generated by transgenic approaches, gene editing, chemical/radiation-based mutagenesis and hybridization. For transgenic lines, describe the transformation method, the number of independent lines analyzed and the generation upon which experiments were performed. For gene-edited lines, describe the editor used, the endogenous sequence targeted for editing, the targeting guide RNA sequence (if applicable) and how the editor was applied.*
Authentication	*Describe any authentication procedures for each seed stock used or novel genotype generated. Describe any experiments used to assess the effect of a mutation and, where applicable, how potential secondary effects (e.g. second site T-DNA insertions, mosiacism, off-target gene editing) were examined.*